HHS Public Access

Author manuscript

*J Immunol*. Author manuscript; available in PMC 2024 May 30.

Published in final edited form as:

*J Immunol*. 2021 May 01; 206(9): 2170–2183. doi:10.4049/jimmunol.2001459.

# Kdm6b Regulates the Generation of Effector CD8+ T Cells by Inducing Chromatin Accessibility in Effector-Associated Genes

**Tianhao Xu**[*,†], **Alexander Schutte**[*], **Leandro Jimenez**[‡], **Andre N. A. Gonçalves**[‡], **Ashleigh Keller**[*], **Matthew E. Pipkin**[§], **Helder I. Nakaya**[‡], **Renata M. Pereira**[¶], **Gustavo J. Martinez**[*,†]

[*]Center for Cancer Cell Biology, Immunology and Infection, Chicago Medical School, Rosalind Franklin University of Medicine and Science, North Chicago, IL

[†]Discipline of Microbiology and Immunology, Chicago Medical School, Rosalind Franklin University of Medicine and Science, North Chicago, IL

[‡]Department of Clinical Analyses and Toxicology, School of Pharmaceutical Sciences, University of Sao Paulo, Brazil

[§]Department of Immunology and Microbiology, The Scripps Research Institute, Jupiter, FL

[¶]Instituto de Microbiologia Prof. Paulo de Goes, Universidade Federal do Rio de Janeiro, Rio de Janeiro, RJ, Brazil

## Abstract

The transcriptional and epigenetic regulation of $CD8^+$ T cell differentiation is critical for balancing pathogen eradication and long-term immunity by effector and memory CTLs, respectively. In this study, we demonstrate that the lysine demethylase 6b (Kdm6b) is essential for the proper generation and function of effector $CD8^+$ T cells during acute infection and tumor eradication. We found that cells lacking Kdm6b (by either T cell−specific knockout mice or knockdown using short hairpin RNA strategies) show an enhanced generation of memory precursor and early effector cells upon acute viral infection in a cell-intrinsic manner. We also demonstrate that Kdm6b is indispensable for proper effector functions and tumor protection, and that memory $CD8^+$ T cells lacking Kdm6b displayed a defective recall response. Mechanistically, we identified that Kdm6b, through induction of chromatin accessibility in key effector-associated gene loci, allows for the proper generation of effector CTLs. Our results pinpoint the essential function of Kdm6b in allowing chromatin accessibility in effector-associated genes, and identify Kdm6b as a potential target for therapeutics in diseases with dysregulated effector responses.

Cytotoxic T lymphocytes, also known as $CD8^+$ T cells, are an essential part of the adaptive immune system designed to eliminate intracellular pathogens and to mediate tumor immune

Address correspondence and reprint requests to Dr. Gustavo J. Martinez, Center for Cancer Cell Biology, Immunology and Infection, Rosalind Franklin University of Medicine and Science, Chicago Medical School, North Chicago, IL 60064. gustavo.martinez@rosalindfranklin.edu.

The sequences presented in this article have been submitted to the Gene Expression Omnibus (http://www.ncbi.nlm.nih.gov/geo/) under accession number GSE161842.

Disclosures

The authors have no financial conflicts of interest.

surveillance. Naive $CD8^+$ T cells are activated upon recognizing their cognate Ag presented by APCs and rapidly proliferate and adopt distinct fates with various effector and memory potential (1, 2). At the peak of the immune response, $CD8^+$ T cells differentiate into a heterogeneous population consisting mainly of two distinct fates: 1) terminally differentiated short-lived effector T cells (SLECs), which are primarily responsible for eliminating the acute infection, and 2) memory precursor effector cells (MPECs) that will give rise to long-lived memory CTLs (1, 3, 4). After resolution of the infection, most Ag-specific terminally differentiated effector CTLs undergo apoptosis because of a lack of Ag stimulation. The remaining $CD8^+$ T cells will form the long-lasting memory pool for durable protection upon subsequent reinfections.

The transcriptional regulation involved in the fate commitment of $CD8^+$ T cells upon their activation has been widely studied (1). The heterogeneity of $CD8^+$ T cells during differentiation is governed and reinforced by several key transcription factors that form a complex regulatory network (2, 5). However, the specific relationship between these fate-governing transcription factors and epigenetic regulators that co-orchestrate $CD8^+$ T cell differentiation remains elusive. Effector CTL differentiation is favored by the combined activity of transcription factors Batf, Irf4, T-bet (encoded by *Tbx21*), Id2, Blimp-1 (encoded by *Prdm1*), Zeb2, and NFAT1, whereas Eomes, Id3, Zeb1, Bcl-6, Tcf-1 (encoded by *Tcf7*), Runx3, and NFAT2 are known transcription factors in driving proper memory $CD8^+$ T cell formation. The relative ratios or abundances of transcription factors within the same family favor the generation of one population over the other. For instance, T-bet and Eomes both belong to the T-box transcription factor family, and a higher T-bet/ Eomes ratio favors the generation of effector CTLs, whereas a lower ratio promotes memory CTLs (6–8). Similarly, whereas Id2 favors effector cell differentiation, Id3 programs memory CTL generation (9–11). Moreover, we have found that NFAT1 is essential for proper effector cell generation, whereas NFAT2 is vital for memory cells (12). Batf and Irf4 have been shown to act as pioneer transcription factors in Th17 cell generation (13) and have also been demonstrated to regulate early effector CTL gene program expression (14). More recently, Runx3 was shown to be an important regulator of memory CTL generation by establishing chromatin accessibility on *cis*-regulatory regions (15) as well as also regulating tissue residency in tumors and nonlymphoid tissues (16).

Although recent research has focused primarily on the role of transcription factors in the generation of effector or memory CTLs (1), the cell-intrinsic changes at the epigenetic level are not fully understood (1, 17, 18). Epigenetic regulation includes DNA methylation, long-noncoding RNA interaction, and covalent modifications of histone residues. Histone modifications such as acetylation, methylation, sumoylation, phosphorylation, and ubiquitination play important roles in regulating gene expression (2, 19). For instance, inactive *loci* are marked by repressive trimethylated histone 3 lysine 27 (H3K27me3) residues (20), whereas H3K4me3 marks are associated with active gene expression. Bivalent deposition of H3K4me3 and H3K27me3 on the same locus is considered to poise gene expression, allowing for adequate temporal regulation of these genes in the presence of the appropriate signals (21). In naive CTLs, many genes critical for lineage commitment, differentiation, metabolism, and cell proliferation possess bivalent H3K4me3 and H3K27me3 marks. Upon naive T cell activation, the repressive H3K27me3

and permissive H3K4me3 marks are extensively changed, facilitating the differentiation of CTLs into effector and memory cells (22–24). Although chromatin dynamics of naive T cell activation are directly associated with transcriptional control of gene expression and T cell lineage commitment (25), the exact molecular mechanisms governing this process are still elusive.

Terminal effector (TE) CTL differentiation requires the repression of pro-memory and pro-survival genes, mediated by polycomb repressive complex 2 (PRC2) catalytic component enhancer of zeste homolog 2 (Ezh2) through trimethylation of H3K27 residues in these loci (22, 26). Dynamic regulation of H3K27me3 levels can be achieved not only through the deposition of this repressive mark by PRC2, but also upon its removal by lysine demethylase 6a (Kdm6a) or 6b (Kdm6b) (27, 28). Demethylation of H3K27 residues is associated with opening of the chromatin structure and deposition of active marks leading to the induction of gene transcription (27). Recently, Yamashita and colleagues have indicated that Kdm6a regulates the generation of effector $CD8^+$ T cells during *Listeria monocytogenes* infection by removing H3K27me3 repressive marks from the *Prdm1* gene locus (29). Although Kdm6b and Kdm6a are both H3K27 demethylases and have high homology in their JmjC domains, their N-terminal domains are less conserved. Some reports have suggested deficiency in Kdm6a or Kdm6b can result in opposite phenotypes, indicating they may even have contrasting functions (30, 31). Kdm6a and Kdm6b were found to be necessary for NKT cell development (32), $CD4^+$ T cell trafficking, and differentiation and function of Tfh and Th17 cells (33–36). However, the role of Kdm6b during $CD8^+$ T cell differentiation is still unclear. In this study, using T cell−specific Kdm6b knockout (KO) mice and short hairpin RNA (shRNA)−mediated knockdown of Kdm6b strategies, we demonstrate that cell-intrinsic Kdm6b-dependent remodeling of chromatin accessibility is indispensable for the proper generation and function of effector CTLs in vivo. We characterized the transcription profile of Kdm6b-deficient $CD8^+$ T cells and found impairment in the induction of effector-associated genes, as well as the cytotoxicity program. Kdm6b-deficient cells show reduced killing activity both in vitro and in vivo. We also observed that although Kdm6b deficiency does not impair the early proliferation of Ag-specific $CD8^+$ T cells during a primary response, it severely impacts the expansion and effector cell differentiation upon secondary challenge. Our results have important implications in the therapeutic manipulation of effector CTL responses during health and disease.

## Materials and Methods

### Mice

All mice were on a C57BL/6J background. The experimental mice were 6- to 8-wk-old and sex- and age-matched. P14 Thy1.1 and CD4-Cre mice have been previously described (12). $Kdm6b^{fl/fl}$ mice were purchased from Jackson Laboratory [stock no. 029615, generated by Dr. Boselut (34)] and bred to create the following genotypes: $Kdm6b^{fl/+}$ CD4-Cre, $Kdm6b^{fl/fl}$ CD4-Cre, P14 Thy1.1 and/or Thy1.2 $Kdm6b^{fl/fl}$ CD4-Cre. Specific lack of Kdm6b protein expression in thymocytes from $Kdm6b^{fl/fl}$ CD4-Cre mice was reported by Dr. Boselut's group (34). We observed 85−90% reduction in Kdm6b mRNA levels from purified $CD8^+$ T cells from day 4 (d4) lymphocytic choriomeningitis virus

(LCMV)−infected animals (Supplemental Fig. 3F). All mice were maintained in specific pathogen−free barrier facilities and used according to protocols approved by the Rosalind Franklin University of Medicine and Science Institutional Animal Care and Use Committee.

## T cells isolation, culture

Naive or total $CD8^+$ cells were purified from spleen and lymph nodes using the Mouse Naive $CD8^+$ T Cell Isolation Kit (catalog no. 19858) or Mouse $CD8^+$ T Cell Isolation Kit (catalog no. 19853) from StemCell Technologies, respectively. DMEM supplemented with 10% heat-inactivated FBS, 2 mM L-glutamine, penicillin-streptomycin, nonessential amino acids, sodium pyruvate, vitamins, 10 mM HEPES, and 50 uM 2-ME were used for T cell culture (37). For T cell activation, naive $CD8^+$ T cells were activated with anti-CD3 (clone 2C11) and anti-CD28 (clone 37.51) (1 μg/ml each, both from BioXcell) and 50 ng/ml gentamicin at 1 million cells per milliliter on a 6-well plate that had been precoated with 50 μg/ml goat anti-hamster IgG (Pierce Protein Biology, Life Technologies). Cells were removed from the initial stimulus 48 h after activation and were cultured at 0.5 million/ml with 100 or 10 U/ml of recombinant human IL-2 (38).

## Retroviral plasmids and transductions

Retroviral particles were generated by transfecting PlatE cells with Ametrine-expressing murine retroviral vectors containing shRNAs targeting CD4 or Kdm6b as previously described (39). Virus supernatant was filtered through 0.45-μm filters and concentrated by centrifugation at 6000 × *g* (F14–14 × 50cy rotor) at 6°C overnight. In vitro−activated $CD8^+$ T cells (as described above) were transduced with retroviral particles 18−20 h after activation. T cell culture media was carefully replaced with media containing concentrated retrovirus supplied with 8 μg/ml polybrene and centrifuged at 2,000 rpm for 1 h at 37°C and then put into 37°C 10% $CO_2$ incubator for 4h. For adoptive transfer of transduced P14 cells, T cell cultures were immediately harvested. For in vitro culture experiments, the original T cell media was used to exchange the added media containing retrovirus, and cells were then expanded until day 6 (d6).

## LCMV models, Listeria infection and plaque assay

Mice were infected i.p. with $2 \times 10^5$ PFUs of LCMV Armstrong (LCMV Arm) and analyzed on d4, day 8 (d8), or day 30 (d30)−day 45 (d45) postinfection (p.i.). For adoptive transfer experiments with transduced CTLs, congenic C57BL/6 (Thy1.2) mice received in vitro−transduced P14 Thy1.1 cells (expressing shCD4 or shKdm6b) and were subsequently infected i.p. with $1.5 \times 10^5$ PFUs of LCMV clone13, as previously described (39). LCMV strains were initially provided by Dr. Shane Crotty at La Jolla Institute and expanded with BHK cells as described (40). Serum viral titers were measured by plaque assay as described (41).

For *L. monocytogenes*−GP33 (LM-gp33) infection, naive P14 wild-type (WT) and Kdm6b KO $CD8^+$ T cells were isolated, activated, and cultured in vitro for 6 d using 10 U/ml rhIL-2. A total of $2.5 \times 10^5$ cells of each genotype were injected (i.v.) into different groups of 5−6-wk-old WT C57BL/6 recipients. Mice with or without transferred cells were then infected (i.v.) with $5 \times 10^4$ CFUs of LM-gp33 the next day. Mice were sacrificed 3 d

p.i. Splenocytes were harvested, and serial dilutions were made with a final concentration of Triton X-100 0.5% before plating on brain-heart infusion plates as described (42). For LM-gp33 rechallenge, $1 \times 10^6$ CFUs were transferred into mice previously infected with LCMV, and mice were euthanized 4 d after challenge. Splenocytes were harvested and phenotypically characterized by FACS, and bacterial burden determined as described above.

## Flow cytometry analysis

Spleens, thymus, lymph nodes, and heparinized blood were used for isolating single-cell suspension. RBCs were lysed from spleens and heparinized blood with ACK lysis buffer. For LCMV tetramer staining, $H^2D^b$-$gp_{33–41}$ (KAVYNFATC) Alexa647 or APC were incubated at room temperature before staining for cell surface molecules and intracellular staining. Cytokine production was measured by FACS from ex vivo splenic cells or in vitro cultured cells (in cytotoxicity assay) upon restimulation with 0.2 μg/ml gp33–41 peptide for 4 h in the presence of brefeldin A. The Abs used in staining are listed in Supplemental Table I. Samples were run on LSRII (BD Biosciences), and data were analyzed with FlowJo (Version 9.9.4 and Version 10.7.1).

## Cytotoxicity assay and tumor protection model

For cytotoxicity assay, naive P14 $CD8^+$ T cells were activated in vitro, transduced with retroviral constructs expressing shRNAs targeting Kdm6b or CD4, and cultured with 10 U/ml rhIL-2 as described above. On d6, $Ametrine^+$ cells were purified by FACS and cocultured at different ratios with GFP-expressing parental mammary carcinoma cell line EO771 (negative control to determine nonspecific target lysis), or EO771 cells expressing the cognate Ag gp33–41 (EO771-GFP-gp33–41) (12). After overnight incubation (~18 h), the remaining live GFP-expressing EO771 cells were determined by flow cytometry as a measure of the cytotoxic activity. EO771 cells cultured in the absence of CTLs were used as a baseline for cell death.

For in vivo tumor protection model, $2 \times 10^6$ EO771-GFP-gp33–41 cells were s.c. injected into C57BL/6 recipient mice. Three days after tumor inoculation, tumor size was measured using a caliper and mice were assigned to experimental groups to normalize their tumor size. A total of $5 \times 10^5$ shRNA-transduced $Ametrine^+$−sorted P14 $CD8^+$ T cells were injected i.v. into those tumor-bearing mice in different groups. Tumor size then measured every other day using a caliper. The tumor volume was determined using the following formula: Width(W)*Width(W)*Length(L)/2. For TILs analysis, $1 \times 10^6$ sorted cells were transferred to tumor-bearing mice (11 days) for 48 h. Tumors were isolated and trenched into pieces smaller than 1 $mm^2$ and incubated in digestion solution (1.5 mg/ml collagenase D and 50 U/ml recombinant DNase I in PBS) and incubated in 37°C for 45 mins with mixing in between incubation. RBC lysis was performed using ACK lysis buffer and then cells were counted and characterized by flow cytometry.

## Mixed adoptive transfer model and lung tissue analysis

Peripheral naive P14 Thy1.1 WT and Thy1.1/Thy1.2 Kdm6b KO cells $CD8^+$ T cells were isolated and mixed in a 1:1 ratio, and $5 \times 10^3$ cells adoptively transferred into C57BL/6-congenic (Thy1.2) recipient mice. Purity of naive cells ($CD8^+$ $CD44^-$ $CD62L^+$) as well

as Thy1.1:Thy1.1/Thy1.2 ratio was confirmed by flow cytometry prior to cell transfer. One day later, mice were infected with LCMV Arm virus. To determine tissue-resident memory T cells in lung, and distinguish from vascular-associated $CD8^+$ T cells, 1 μg of anti-CD8β PerCP-Cy5.5 Ab per mouse was injected i.v. three minutes prior to euthanasia and lung tissue extraction, as previously described (16). $CD8\beta^-$ cells were considered to be localized within nonlymphoid tissues. Lungs were cut into pieces smaller than 1 $mm^2$ and incubated in digestion solution (1.5 mg/ml collagenase D and 50 U/ml recombinant DNase I in PBS) and incubated in 37°C for 30 min with mixing in between incubation. Digestion was neutralized by adding T cell media and tissues further dissociated over a 70-μm nylon cell strainer (VWR). Then lymphocytes were purified using a 40:60% Percoll density gradient separation. Spleens were also harvested from each mouse, and single-cell suspensions were generated. RBC lysis was performed using ACK lysis buffer, after which isolated cells were characterized by flow cytometry.

### Mix bone marrow reconstitution and infection

Bone marrow cells were isolated from the tibia and femur. Mixed bone marrow chimera mice were generated by adoptive transfer of 1:1 or 1:5 ratio of bone marrow cells from B6.SJL ($CD45.1^+$) mice and bone marrow cells from either Kdm6b T cell−specific (TKO) or WT ($CD45.2^+$) mice into lethally irradiated B6.SJL mice (total of $7 \times 10^6$ bone marrow cells). After 6 wk, reconstitutions were checked via bleeding and mice were then infected with LCMV Arm strain ($2 \times 10^5$ PFUs per mouse). Eight days p.i., mice were euthanized, and expression of KLRG1, CD127, and CXCR3 was determined on $CD8^+$ $CD44^{hi}$ $CD4^-$ $B220^-$ $H2D^b$-$gp_{33–41}{}^+$ Ag-specific splenic cells (both in $CD45.1^+$ and $CD45.2^+$ populations).

### RT-PCR and quantitative real-time RT-PCR

Total RNA was isolated from FACS-purified $CD8^+$ T cells using TRIzol reagent (Invitrogen) according to manufacturer's instructions. Superscript reverse transcriptase (Invitrogen) and oligonucleotide primers were used to synthesize cDNA. Gene expression was examined with 7900 Real Time PCR System (Applied Biosystems) using Power SYBR green PCR Master Mix (Thermo Fisher Scientific). Gene expression was normalized to *Rpl32* (encodes L32 ribosomal protein) gene expression. The following primers were used: *Rpl32* forward, 5′-CGTCTCAGGCCTTCAGTGAG-3′; *Rpl32* reverse, 5′-CAAGAGGGAGAGCAAGCCTA-3′; *Prdm1* forward, 5′-TGCGG AGAGGCTCCACTA-3′; *Prdm1* reverse, 5′-TGCGGAGAGGCTCCACTA-3′; *Id3* forward, 5′-TGCTACGAGGCGGTGTGCTG-3′; *Id3* reverse, 5′-TGTCGTCCAAGAGGCTAAGAGGCT-3′; *Tcf7* forward, 5′-CAAGGCA-GAGAAGGAGGCTAAG-3′; *Tcf7* reverse, 5′-GGCAGCGCTCTCCTTGAG-3′; *Tbx21* forward, 5′-AGGGGGCTTCCAACAATG-3′; *Tbx21* reverse, 5′-AGACGTGTGTGTTAGAAGCACTG-3′; *Zeb2*(set1) forward, 5′-GGCAA GGCCTTC AAG TACA-3′; *Zeb2*(set1) reverse, 5′-AAGCGTTTCTTG-CAGTTTGG-3′; *Zeb2*(set2) forward, 5′-GAGCAGGTAACCGCAAGTTC-3′; *Zeb2*(set2) reverse, 5′-GATATTGTTTCTCATTCGG-3′; Kdm6b forward, 5′-CCCCCATTTCAGCTGACTAA3′; Kdm6b reverse, 5′-CTGGACCAA GGGGTGTGTT-3′. For RT-PCR, we used the following

primer spanning exons 17−18: Kdm6b forward, 5′-CCATCCTGGGCATGAACACC-3′ and Kdm6b reverse, 5′-CAGAAGGCGCTGATGGTCTC-3′.

## RNA sequencing

FACS-purified cells from in vivo experiments were washed twice with PBS, and $1 \times 10^4$ cells were used for sequencing. cDNA was generated using SMART-seq v4 Ultra Low Input RNA Kit (Takara Bio), followed by Nextera XT (Illumina) library generation according to the manufacturers' instructions. Multiplexed libraries were pooled and run on NovaSeq S1 or S2 flow cells with 50 × 50 pair-end reads.

The paired-end reads that passed Illumina filters were filtered for reads aligning to tRNA, rRNA, adapter sequences, and spike-in controls. The reads were then aligned to mm10 reference genome using STAR (v2.6.1) (43). DUST scores were calculated with PRINSEQ Lite (v 0.20.3) (44) and low-complexity reads (DUST > 4) were removed from the BAM files. The alignment results were parsed via the SAMtools (45) to generate SAM files. Read counts to each genomic feature were obtained with the featureCounts (v 1.6.5) (46) using the default option along with a minimum quality cut off (Phred > 10). After removing absent features (zero counts in all samples), the raw counts were then imported to R/Bioconductor package DESeq2 (v 1.24.0) (47) to identify differentially expressed genes among samples. The $p$ values for differential expression are calculated using the Wald test for differences between the base means of two conditions. These $p$ values are then adjusted for multiple test correction using Benjamini-Hochberg algorithm (48). We considered genes differentially expressed between two groups of samples when the DESeq2 analysis resulted in an adjusted $p$ value < 0.05. Principal component analysis was performed using the 'prcomp' function in R. RNA-sequencing (RNA-seq) differential−expressed genes were plotted on the volcano plot. Further analysis were completed in R. Early effector-versus-effector or TE-versus−memory precursor gene signature (padj < 0.05) data sets were ranked based on their log2FC. Gene symbol or alias from the preranked signature data sets and RNA-seq differential−expressed genes (padj < 0.05) were converted into ENTREZID using clusterProfiler package (Bioconductor) before passing to pathway analysis enrich for biological process or use for gene set enrichment analysis (GSEA) described in clusterProfiler vignette.

## Assay for transposase-accessible chromatin sequencing

Assay for transposase-accessible chromatin sequencing (ATAC-seq) libraries were prepared as described (49). Briefly, $5 \times 10^4$ FACS-purified cells were washed twice with PBS and treated with lysis buffer (10 mM Tris pH 7.5, 10 mM NaCl, 3mM MgCl2, 0.1% NP-40). Pellets were then resuspended with 50 μl of Tn5 transposase containing 1× TD buffer (Nextera DNA Sample Prep Kit, Illumina, San Diego, CA) and incubated for 30 min at 37°C. Genomic DNA was then purified with QiaQuick MinElute PCR Purification Kit (Qiagen, Valencia, CA), and DNA amplified with KAPA HiFi Real-Time Library Amplification Kit (Kapa, Wilmington, MA) according to manufacturer's instructions using barcoded primers for 11−13 cycles. Amplified libraries were purified with QiaQuick MinElute PCR Purification Kit, quantified, and pooled. Pooled libraries were pair-end sequenced on S1 100 flow cell on NovaSeq (Illumina, San Diego, CA) with 50 bp cycles in

each direction. Raw data from the sequencer were uploaded to Illumina basespace (Illumina, San Diego, CA), and the samples were separated based on their barcodes and FASTQ files for each read obtained from each sample.

Sequencing Reads were mapped to the mouse genome (mm10) using bowtie (50) (-p 15 -m 1 −best - strata -X 2000 -S−fr−chunkmbs 1024). BAM files from replicates of WT and KO were merged and processed with picard MarkDuplicates to identify duplicate reads. Then, duplicate reads, mitochondria DNA, Y chromosome DNA, and fragments larger than 100 bp were excluded by SAMtools (45). Coordinates of reads were then shifted (plus strand +4, minus strain −5). Fragments were used to call peak summits with MACS2 (51) using parameters "−nomodel -q 0.01−keep-dup all−call-summits." The summits for each peak from all replicates were expanded to regions with a uniform size of 500 bp. We excluded regions that intersected ENCODE-blacklisted regions for mm10 using trackerlayer R package.

We identified the Tn5 insertion site by isolating the first 9bp of each read and computed the number of transposase insertions per peak for each replicate with bedtools coverage (version 2.16.2) (52). Counts of ATAC-seq peaks were generated for all replicates and samples using featureCounts from the Rsubread R package (countMultiMappingReads = FALSE,maxFragLength = 100). Raw ATAC-seq counts in each peak for all replicates of all samples were normalized between replicates with size factors computed with DESeq2 (47) to differential coverage. Pairwise contrasts were performed with DESeq2 and differentially accessible regions were filtered based on a false discovery rate (padj) value of less than 0.05 and −0.5 > log2fc > 0.5. All bedgraph files of ATAC-seq or chromatin immunoprecipitation sequencing (ChIP-seq) are normalized by multiplying counts to a scaling factor calculated by $10^9$/accumulation-factor (accumulation-factor calculation: awk '{sum+=(($3-$2)*$4)} END {print sum}'). Bedgraph files were transformed to bigwig by bedgraphtobigwig, and uploaded as UCSC custom tracks. H3K27me3 ChIP-seq was obtained from GSE89036 (26).

### Statistics and analysis

Graphs were plotted using Prism 7 and 8 GraphPad. Statistical analysis was performed using nonpaired one-way ANOVA followed by Tukey multiple comparisons, two-tail paired or nonpaired Student *t* test, or two-way ANOVA followed by Dunnett comparisons.

## Results

### Kdm6b is required for effector CD8$^+$ T cell differentiation throughout acute viral infection

Kdm6a and Kdm6b are essential for proper development, as demonstrated by the embryonic or neonatal lethality of germline KO mice (53, 54). By using T cell−specific deficiency of both Kdm6a and Kdm6b, Bosselut and colleagues have shown the crucial role of Kdm6 members in T cell development (34). To study the role of Kdm6b in CTL differentiation, we bred Kdm6b-floxed with CD4-Cre mice and generated Kdm6b$^{fl/fl}$ CD4Cre (Kdm6b T cell-specific KO, in this study referred to as Kdm6b TKO) or Kdm6b$^{fl/+}$ CD4Cre (T-Het) mice. Our data, similar to previously published reports (33, 34), showed that Kdm6b TKO mice have an increase in the percentage and numbers of both mature CD4 and CD8

single-positive cells compared with WT mice in the thymus (data not shown). Similarly, we also identified a concomitant reduction in peripheral T cells with $CD4^+$ T cells being more affected than $CD8^+$ T cells, implicating a partial defect of mature T cell egress (data not shown). Moreover, no defects, and in fact somewhat higher regulatory T cells frequencies among $CD4^+$ T cells were observed in spleen and lymph nodes of Kdm6b TKO mice compared with WT controls (data not shown). Our data are consistent with previous publications suggesting that Kdm6b contributes to proper T cell development and that this phenotype is independent of housing or possible microbiota differences across institutions (33).

To comprehend the requirement of Kdm6b in the fate decision toward effector and memory $CD8^+$ T cell differentiation upon an acute infection, we infected WT, Kdm6b T-Het, and Kdm6b TKO mice with LCMV Armstrong strain. We found that the frequency and numbers of total $CD8^+$ T cells as well as Ag-specific $CD8^+$ T cells (determined using $H2D^b$-$gp_{33–41}$ tetramers), were similar between all groups on d8 p.i. (Supplemental Fig. 1A–D). These results suggest that Kdm6b deficiency does not impair $CD8^+$ T cell expansion, proliferation, and/or survival during a primary immune response. We then assessed the generation of effector and memory CTLs by measuring KLRG1 and CD127 (IL-7Rα) expression in Ag-specific cells. We found that Kdm6b TKO mice showed a significant reduction in TEs, and a concomitant increase in memory precursor and early effector cells (EECs) in terms of frequency and total numbers (Fig. 1A–C). We also observed an increase in CXCR3-expressing Ag-specific cells in Kdm6b TKO mice compared with WT and T-Het control mice, providing further evidence of the enhanced preference toward memory precursor cell generation (Supplemental Fig. 1E–F). We then assessed whether Kdm6b TKO mice were able to properly control the acute viral infection by assessing viral titers in serum. We found all experimental groups displayed no detectable viral plaques (data not shown), suggesting that despite reduced effector CTL generation, Kdm6b TKO mice are able to control a primary acute viral infection.

Given the observed increase in EEC and memory precursor cells in Kdm6b TKO mice compared with WT controls, we then assessed the expression of key transcription factors that regulate effector $CD8^+$ T cell differentiation. We found the expression of T-bet, Eomes, and Blimp-1 were significantly lower in CTLs from Kdm6b TKO mice compared with the T-Het or WT control, suggesting their plausible contribution to the reduction in the TE cell population (Fig. 1D, 1E). A similar reduction in T-bet and Eomes expression was observed in distinct populations based on KLRG-1 and CD127 expression (data not shown). To comprehend whether Kdm6b deficiency leads to impaired CTL function, we measured cytokine production upon restimulation of splenocytes with the gp33–41 peptide. Despite decreased numbers of TE cells, Kdm6b-deficient Ag-specific cells showed a higher frequency of IFN-$\gamma^+$ TNF-$\alpha^+$−producing cells (Fig. 1F), although there were no differences in total cytokine-producing Ag-specific cell numbers compared with the controls (Supplemental Fig. 1G). Overall, these results suggest that Kdm6b deficiency does not result in defective polyfunctional IFN-$\gamma^+$ and TNF-$\alpha^+$ production in CTLs.

Our data, together with previously published reports, show that depletion of Kdm6a or Kdm6b in T cells results in reduced splenic CD4 T cells [data not shown and (34)]. It has

also been demonstrated that in the context of chronic viral infection, mice with a deficiency of Kdm6a in T cells show decreased follicular helper T (Tfh) cell development (55). Thus, we next determined if Kdm6b is necessary for the proper generation of Tfh cells in the context of an acute viral infection. Eight days after LCMV Arm infection, we found a reduction of total $CD4^+$ T cells as well as Tfh cells ($CD4^+$ $PD\text{-}1^+$ $CXCR5^+$) in spleens (Supplemental Fig. 1H). Similarly, mixed bone marrow chimera experiments also showed that Kdm6b-deficient cells differentiated to a lesser extent into Tfh cells compared with WT controls (data not shown). Thus, our results demonstrated a cell-intrinsic role of Kdm6b in driving Tfh cell generation upon acute viral infection. We observed no difference between Kdm6b T-Het mice and WT controls in any of the markers measured, suggesting Kdm6b haploinsufficiency is sufficient for proper T cell differentiation (Fig. 1, Supplemental Fig. 1). For this reason, for the remainder of this work, we excluded any further analysis on Kdm6b T-Het mice.

## Kdm6b deficiency results in impaired secondary responses despite sustained memory phenotype

Our results suggest that deficiency in Kdm6b enhances the generation of memory precursor cells at the peak of the acute viral infection (Fig. 1). To determine whether this response is sustained at later time points, we analyzed mice at d45 after LCMV Arm infection (Fig. 2A). Similar to our previous observation, we demonstrate that mice with a T cell−specific deletion of Kdm6b showed significantly enhanced $CD127^+$ $KLRG1^-$ memory cells and $CXCR3^+$ $KLRG1^-$ cells, as well as a concomitant decrease in $KLRG1^+$ effector memory cells (Fig. 2B, 2C). The total number of splenocytes as well as the number and frequency of total $CD8^+$ T cells were similar between experimental groups (data not shown). However, the frequency and number of $H2D^b\text{-}gp_{33–41}{}^+$ Ag-specific cells were significantly higher in Kdm6b TKO mice than the WT group (Supplemental Fig. 2A). We then determined the expression of transcription factors and found a significant reduction in Eomes expression despite observing an increase in the memory subset (Supplemental Fig. 2D). Upon restimulation with gp33–41 peptide, we observed higher frequencies of IFN-γ− and TNF-α−producing cells (Fig. 2D, 2E) but comparable numbers of cytokine-producing cells (Supplemental Fig. 2E), similar to what we have identified at the peak of the immune response in d8 p.i.

To determine whether the enhanced generation of memory cells in Kdm6b TKO mice correlates with enhanced recall responses, d45 LCMV-infected mice were challenged with *L. monocytogenes* expressing gp33–41 epitope as previously described (56). Four days p.i., splenocytes were harvested and $H2D^b\text{-}gp_{33–41}{}^+$ Ag-specific $CD8^+$ T cells were further characterized. The frequency and number of Ag-specific cells was higher in Kdm6b TKO mice compared with controls at a memory time point from a primary infection (d45) (Supplemental Fig. 2A). However, upon rechallenge with LM-gp33, we observed a reduction in $H2D^b\text{-}gp_{33–41}{}^+$ Ag-specific cells compared with WT counterparts (Supplemental Fig. 2F). Consistently, only the WT mice reacquired KLRG1 expression on Ag-specific cells, indicative of a secondary stimulation of Ag-experienced cells, whereas Kdm6b TKO mice failed to re-express effector-associated marker KLRG1. Instead, Ag-specific $CD8^+$ T cells in the Kdm6b TKO mice maintained a higher expression of memory-

associated markers CD127 and CXCR3 (Fig. 2F, 2G, Supplemental Fig. 2G), suggesting Kdm6b is essential for the proper expansion and effector differentiation of Ag-specific cells during a recall response.

## Cell-intrinsic role of Kdm6b in effector CTL generation and memory population maintenance

To evaluate whether Kdm6b induces effector CTL differentiation in a cell-intrinsic manner, we generated mixed bone marrow chimeras by mixing CD45.1 WT bone marrow cells with either WT or Kdm6b TKO CD45.2 bone marrow cells in a 1:1 ratio and cotransferred into lethally irradiated B6.SJL ($CD45.1^+$)-congenic recipient mice (Supplemental Fig. 3A). Mice were infected with LCMV Arm 6 wk after bone marrow transfer, and then cells characterized on d8 p.i. We determined the ratio of CD45.1 versus CD45.2 lymphocytes in the blood (prior to infection) and in spleens (p.i.) and found fewer Kdm6b-deficient $CD4^+$ and $CD8^+$ T cells compared with controls (around 5:1 ratio of CD45.1 versus CD45.2), but more B cells (around 1:2 ratio of CD45.1 versus CD45.2) in each case, suggesting Kdm6b-deficient T cells were outcompeted by their WT counterparts (Supplemental Fig. 3B, 3C). Upon LCMV infection, we observed a similar decrease in SLECs and an increase in memory precursors and EECs in Kdm6b-deficient cells compared with WT controls (Supplemental Fig. 3D, 3E). Because of the seemingly competitive disadvantage of Kdm6b-deficient T cells compared with WT counterparts, we also performed mixed bone marrow chimeras by mixing Kdm6b TKO ($CD45.2^+$) and WT ($CD45.1^+$) bone marrow cells in a 5:1 ratio. Six weeks after reconstitution, a comparable ratio of WT to Kdm6b KO $CD4^+$ and $CD8^+$ T cells was observed in these experiments (data not shown). These data suggest that the competitive advantage of WT cells can be leveled by enhancing the initial frequency of Kdm6b-deficient precursor cells. In these settings, Kdm6b-deficient cells were still defective in committing to an effector fate upon acute viral infection, similar to the results observed in the 1:1 ratio of BM transfer (data not shown).

To further assess if Kdm6b deficiency leads to reinforced memory $CD8^+$ cell generation, we used a mixed adoptive transfer model of P14 TCR-transgenic T cells, which recognize the gp33–41 epitope of LCMV. The advantage of this model consists of the fact that both WT and Kdm6b-deficient T cells are exposed to the same viral load and inflammatory condition in the same recipient mice. For this purpose, we isolated naive P14 Thy1.1 WT and P14 Thy1.1/Thy1.2 Kdm6b-deficient $CD8^+$ T cells, mixed them in a 1:1 ratio and transferred them into C57BL/6-congenic (Thy1.2) recipient mice, which were subsequently infected with LCMV Arm (Fig. 3A). Although the frequency of Kdm6b-deficient cells were slightly higher on day 0, upon infection, the WT cells outcompeted the Kdm6b-deficient cells (both at the peak of the immune response on d8 or at memory time points past d30) (Fig. 3B, 3C). Together with the mixed bone marrow experiments, our results indicate a two-layer competition disadvantage of Kdm6b-deficient T cells: 1) in the generation of peripheral naive $CD8^+$ T cells and 2) in the expansion of activated T cells during acute viral infection.

When assessing the generation of effector and memory CTLs in the mixed adoptive transfer experiment, we found that $CD8^+$ T cells lacking Kdm6b preferentially committed to a memory fate with reduced effector cell generation both at the peak of the immune response

on d8 as well as memory time points (Fig. 3D, 3E, Supplemental Fig. 3G, 3H). We also observed that roughly 20% more $CD8^+$ T cells lacking Kdm6b become central memory CTLs (Tcm), compared with WT controls, by measuring expression of CD62L, CD127, and CXCR3 (Fig. 3E, Supplemental Fig. 3H). Similarly, we detected decreased T-bet but increased Eomes and Tcf-1 expression in Kdm6b-deficient splenic CTLs (Fig. 3F). The expression pattern of these transcription factors supports the enhanced memory phenotype, especially the central memory population. We then investigated whether the preferred commitment of Kdm6b-deficient T cells toward Tcm resulted in impaired tissue-resident memory cell generation or maintenance (Supplemental Fig. 3I). For this purpose, we i.v. injected an Ab against CD8β prior to euthanasia to distinguish cells in circulation versus tissue-resident cells, which would not be stained by CD8β. We found decreases in both the frequency of Kdm6b-deficient lung resident memory $CD8^+$ T cells (Trm), as well as in the expression of the activation and tissue-resident marker CD69 in those cells compared with WT controls (Supplemental Fig. 3I). Our data suggest that Kdm6b deficiency promotes Tcm generation while reducing the Trm population. Although, it is plausible that the impaired Trm cell generation in Kdm6b-deficient cells might be a secondary effect because Trm cells have the potential to differentiate not only from MPECs but also from SLECs (“ex-KLRG1 cells”) as recently demonstrated (57). Altogether, we identified that Kdm6b supports effector and Trm cell differentiation, and restricts Tcm generation in a cell-intrinsic manner that largely echoes the phenotype observed upon infection of Kdm6b TKO mice.

To further comprehend the role of Kdm6b during recall responses, mice receiving the adoptively transferred cells were rechallenged with LM-gp33 on d45. Four days later, mice were euthanized, and the phenotype of WT and Kdm6b-deficient cells assessed (Fig. 3A). We found, similar to the observations in Kdm6b TKO mice (Fig. 2), a reduction in the expansion of Kdm6b-deficient cells compared with their WT counterparts (day 49, Fig. 3B, 3C). Although WT P14 cells reacquired KLRG1 expression upon secondary challenge, Kdm6b-deficient P14 cells maintained high levels of CD127 and CD62L expression, indicative of enhanced central memory cells (Fig. 3G, Supplemental Fig. 3J). Upon rechallenge, we observed similar increase in T-bet and decrease in Tcf1 expression as observed at memory time points (d30) (Fig. 3H). Consistent with the decrease in expansion of Kdm6b KO cells, we observed decrease Ki67 levels compared with WT controls (Fig. 3I), indicating that Kdm6b-deficient cells have a defective proliferative response upon recall responses. Therefore, these results confirm that Kdm6b, unlike Kdm6a (29), is essential for mounting secondary responses in $CD8^+$ T cells in a cell-intrinsic manner.

## Acute deletion of Kdm6b results in decreased effector CTL generation and effector-associated gene expression

Kdm6b is deleted during T cell development at the $CD4^+$ $CD8^+$ double-positive stage in Kdm6b TKO mice, which could result in abnormal differentiation or compensatory mechanisms during T cell development or homeostasis. Thus, we next determined whether acute deletion of Kdm6b upon T cell activation using an shRNA strategy would also impact effector CTL commitment. For this purpose, WT $Thy1.1^+$ P14 TCR-transgenic $CD8^+$ T cells were activated in vitro with anti-CD3 and anti-CD28 Abs and transduced with retroviral constructs (expressing Ametrine) containing shRNA against Kdm6b (or

CD4 as control). Cells were then transferred into congenic C57BL/6 (Thy1.2) WT mice that were subsequently infected with LCMV, as previously described (39). Eight days p.i., spleens were harvested and transduced donor cells (P14 Thy1.1$^+$ Ametrine$^{hi}$) were analyzed for expression of KLRG1 and CD127 (Fig. 4A). We observed a slight reduction in shKdm6b-expressing cells compared with shCD4 controls, consistent with the competitive disadvantage in the presence of WT cells (Supplemental Fig. 4). Similar to our results using Kdm6b T cell−specific KO mice, we observed a decrease in SLECs but an increase in MPECs and EECs upon Kdm6b deficiency (over 85% knockdown efficiency based on quantitative PCR (qPCR) analysis, Supplemental Fig. 4E), suggesting that acute Kdm6b deficiency during T cell activation affects the proper generation of effector CD8$^+$ T cells in vivo (Fig. 4A, 4B). We also observed increased IFN-γ and TNF-α expression, but Granzyme B production in Kdm6b-deficient cells was drastically reduced compared with controls (Fig. 4C), suggesting that the Kdm6b-dependent CTL effector program can be epigenetically regulated through distinct mechanisms (cytotoxicity versus cytokine production).

To understand the genes regulated by Kdm6b, we performed RNA-seq on FACS-purified P14 Thy1.1$^+$ Ametrine$^{hi}$ cells. We identified 379 upregulated and 253 downregulated genes in the Kdm6b-deficient CTLs compared with shCD4 control (Fig. 4D). We observed an increase in *Cxcr3* expression and decreased *Klrg1* expression in Kdm6b-deficient cells, which corroborates our phenotypic assessments. Within the differentially expressed genes, transcription factors *Tcf7*, *Id3*, and *Eomes*, which are crucial for memory cell generation, were upregulated in Kdm6b-deficient CD8$^+$ T cells. In contrast, effector CTL-promoting transcription factors such as *Id2*, *T-bet*, and *Zeb2* were downregulated in the Kdm6b knockdown CTLs compared with controls. To validate these results, we also performed qPCR with the same sorted cells we used for RNA-seq. Additionally, we found Kdm6b-deficient CTLs displayed decreased expression of *Prdm1*, which is previously known to be regulated by Kdm6a (29) (Supplemental Fig. 4E). Altogether, our data suggest that Kdm6b deficiency derails effector CD8$^+$ T cell differentiation and causes cells to preferentially commit to a memory fate. To confirm this, we next performed GSEA using previously published differentially expressed genes in effector and memory subsets. We determined that effector-associated genes are downregulated in Kdm6b KO cells, whereas memory-associated genes are upregulated in Kdm6b KO cells (Fig. 4E). To further understand what pathways may be impacted by Kdm6b deficiency during differentiation, we performed gene ontology analysis. Pathways related to cell migration, chemotaxis, and cytotoxicity were enriched in genes downregulated upon Kdm6b deficiency in CD8$^+$ T cells (Supplemental Fig. 4F). Taken together, our shRNA-mediated depletion of Kdm6b as well as our T cell−specific Kdm6b KO data indicate that Kdm6b is needed for proper effector and memory signature gene expression upon T cell activation, and also suggest that the CTL effector program can be epigenetically regulated through distinct mechanisms, with Kdm6b being a central regulator of the cytotoxicity program and not cytokine production.

## Kdm6b is required for effector CTL function and tumor control

Our data shows Kdm6b deficiency in CTLs resulted in reduced effector subset differentiation and Granzyme B production but normal IFN-γ and TNF-α polyfunctional

cells compared with Kdm6b-sufficient CTLs. Our RNA-seq pathway analysis also suggests that cell migration and cytotoxicity are significantly impacted by Kdm6b depletion. These findings prompted us to investigate whether Kdm6b deficiency affects cytotoxic activity in a cell-intrinsic manner. For this purpose, we used in vitro−activated shCD4 or shKdm6b transduced memory-like cells as previously described (12). We found that, similar to our in vivo findings, Kdm6b-deficient cells displayed decreased Granzyme B expression and similar or even slightly enhanced IFN-γ and TNF-α production (Supplemental Fig. 5A). To assess their cytotoxic function in vitro, WT or Kdm6b-deficient memory-like P14 $CD8^+$ T cells were cocultured overnight at different ratios with EO771 mammary carcinoma cell line expressing the cognate Ag gp33–41 and GFP (Fig. 5A). We measured $GFP^+$ live cells as a readout for cytotoxicity and found that Kdm6b-deficient cells showed reduced killing capacity upon Ag recognition (Fig. 5B). To confirm that impaired cytotoxicity can be translated in vivo, we used a tumor protection experiment in which we s.c. inoculated EO771-GFP-gp33–41 into naive congenic recipient mice. Three days later, WT (shCD4-expressing) or Kdm6b-deficient P14 T cells, which recognize the gp33–41 epitope expressed by tumor cells, were transferred, and tumor growth was measured every other day (Fig. 5C). We found that whereas cells expressing shCD4 could control tumor growth properly, mice receiving Kdm6b-deficient CTLs were unable to control tumor growth compared with mice that did not receive any cells (Fig. 5D). This lack of tumor control was not caused by impaired T cell infiltration in the tumor, as similar frequencies of WT or Kdm6b-deficient TILs were observed 48 h after T cell transfer (Supplemental Fig. 5B, 5C). Similarly, in vitro−generated Kdm6b-deficient memory-like CTLs were unable to protect mice from *L. monocytogenes* infection (Supplemental Fig. 5C–F). Thus, these results suggest that Kdm6b is indispensable for proper effect- or cytotoxic functions in $CD8^+$ T cells.

## Kdm6b is required for proper chromatin accessibility of effector-associated genes, which correlates with the demethylation of H3K27 residues

To understand the mechanism by which Kdm6b regulates effector cell generation, we performed the mixed adoptive transfer experiment described in Fig. 3A. In this instance, mice were euthanized 4 d p.i., and adoptively transferred cells purified to determine the transcriptional and chromatin accessibility changes observed prior to differentiation of cells into effector and memory CTLs. Although we observed higher frequencies of WT P14 cells compared with Kdm6b KO P14 at d8 or d30 p.i. (Fig. 3B, 3C), we found similar or even slightly higher frequencies and numbers of Kdm6b-deficient cells compared with WT controls at d4 p.i. (Fig. 6A, top panel, and Supplemental Fig. 6A, 6B), suggesting that the competitive disadvantage observed from Kdm6b-deficient cells is because of the proliferative burst from effector CTLs after d4. At this time point, few CTLs were able to commit to the terminally differentiated $KLRG1^+$ fate, whereas most cells remained EECs with no commitment toward the memory precursor fate as measured by CD127 expression (Fig. 6A–C).

To understand the early transcriptional changes regulated by Kdm6b during $CD8^+$ T cell activation in vivo, we performed RNA-seq from WT P14 Thy1.1 and Kdm6b KO P14 Thy1.1 Thy1.2 obtained from the same mice. We observed 200 genes were upregulated in Kdm6b-deficient cells compared with WT counterparts, whereas 88 were significantly

downregulated in Kdm6b-deficient cells (Fig. 6D). Among the genes that were significantly downregulated upon Kdm6b deficiency, we found *Id3*, *Zeb2,* and *Prdm1*, which have been shown to regulate effector CTL differentiation. Moreover, *Il2ra,* which codes for CD25 (high-affinity IL-2R subunit) and *Il12rb1*, the shared subunit between IL-12R and IL-23R, were also downregulated in Kdm6b-deficient cells compared with WT counterparts. It has been previously suggested that IL-2 as well as type I IFNs and IL-12 are important cytokines that drive effector CTL differentiation in part by downregulating expression of TCF-1 among others (8, 38, 58, 59), which could contribute to the phenotypic changes observed in CTLs lacking Kdm6b. To validate that Kdm6b-deficient cells failed to acquire effector-associated signature genes, we performed GSEA. We identified that genes upregulated in Kdm6b-deficient cells were significantly enriched in early effector and memory-associated genes, wheras downregulated genes in Kdm6b KO cells were enriched in effector gene signatures (Fig. 6E). Given that Kdm6b KO cells show reduction in the frequency of $KLRG1^{+}CD127^{-}$ population, we cannot rule out that some of the enriched genes are because of the differences in these populations. However, the $KLRG1^{+}$ population represents a minor percentage compared with EECs ($KLRG1^{-}$ $CD127^{-}$), and therefore our data suggests mostly that the observed enrichment reflects an effect of Kdm6b on these effector genes already in the $KLRG1^{-}CD127^{-}$ population. Thus, our results suggest that Kdm6b is a critical regulator for promoting the expression of effector-associated genes, including transcription factors and cytokine receptors, among others. Altogether, these results indicate Kdm6b is indispensable during early $CD8^{+}$ T cell differentiation for CTLs to transition from EECs to terminally differentiated effector cells.

We then assessed the chromatin accessibility changes that occur early during the $CD8^{+}$ T cell activation/differentiation between WT and Kdm6b KO cells to understand how deficiency in Kdm6b results in preferential inhibition of effector CTL generation. Kdm6b-deficient CTLs surprisingly showed enrichment of 1113 accessible peaks within 1kb of transcription starting site (TSS), which are more likely to be at the promoter and nearby enhancer regions. In contrast, WT control CTLs have 523 enriched accessible peaks within 1kb of TSS (Fig. 6F). To further examine the relationship between chromatin accessibility changes and RNA expression upon Kdm6b deficiency, we plotted the differential gene expression versus ATAC-seq differential peaks. Only regions assigned to genes differentially expressed by RNA-seq are shown. Among those differentially accessible regions determined by ATAC-seq, we observed a positive correlation between open chromatin and upregulated gene expression in each genotype (Fig 6G). We found that Kdm6b-deficient cells displayed correlation between significantly open chromatin accessibility and increased gene expression such as *Tcf7* and *Id3.* Conversely, their WT counterparts displayed significantly increased accessibility in genes like *Klrg1*, *Zeb2*, *Il2ra*, and *Gzmb*, which are known to be associated with effector CTLs. Collectively, these results strongly support that Kdm6b is required for remodeling the accessibility of genes associated with effector $CD8^{+}$ T cell differentiation. Using published H3K27me3 ChIP-seq data from naive and effector CTLs, we investigated the correlation between the differentially accessible regions identified by ATAC-seq and their respective H3K27me3 methylation pattern in naive and effector (TE) $CD8^{+}$ T cells. Within the differentially reduced accessible regions identified in Kdm6b-deficient CTLs compared with WT controls, many of them are demethylated upon activation

and differentiation into effector CTLs. Examples include the promoter regions and some of the distal regions of *Zeb2*, *Klrg1*, *Il2ra*, *Gzmb*, and *Prf1* loci (Fig 6H, Supplemental Fig. 6C). Conversely, *Tcf7* locus, which shows higher accessibility in Kdm6b KO cells compared with their WT counterparts, is associated with increased H3K27me3 marks in effector CTLs compared with naive cells (Supplemental Fig. 6C). Together, our results show that effector-associated gene loci that display demethylated H3K27 residues compared with naive counterparts also show reduced accessibility upon Kdm6b deficiency. Given that we observe enhanced accessibility of memory and early effector genes in Kdm6b KO cells, it is possible that Kdm6b not only directly promotes the accessibility of effector-associated genes, but could also have an indirect effect in the repression of naive- or early effector-associated genes. Overall, these results suggest that Kdm6b is essential for the proper opening of chromatin regions of effector-associated genes from naive $CD8^+$ T cells.

## Discussion

Understanding $CD8^+$ T cell differentiation in response to viral infection and tumor control is critical for novel vaccine development and improving immunotherapy efficacy. The differentiation of CTLs is controlled not only by fate-determining transcription factors but also by epigenetic regulators. Recent studies have demonstrated drastic epigenetic landscape differences among CTL subsets, especially in the deposition of permissive H3K4me3 and repressive H3K27me3 marks, or in DNA methylation status. The epigenetic landscape changes implicate the necessity of epigenetic regulators for proper $CD8^+$ T cell differentiation. Many epigenetic regulators, such as Dnmt3a, Suv39h1, Kdm6a, and Ezh2, were found to promote effector CTL differentiation (22, 26, 29, 60–62). In this study, we confirmed previous studies showing that CD4-Cre driven Kdm6b deficiency in T cells resulted in increased mature single-positive $CD4^+$ and $CD8^+$ T cells (33, 34), and demonstrated that Kdm6b is essential for effector $CD8^+$ T cell differentiation and proper effector function. We also identified a cell-intrinsic role of Kdm6b in the generation of Tfh cells, similar to what has been previously described for Kdm6a (55).

Kdm6a and Kdm6b may have nonredundant and additive effects in $CD8^+$ T cell responses. Several studies have shown that both Kdm6a and Kdm6b are critical for $CD4^+$ T cell egress from the thymus to peripheral lymphoid organs by regulating *S1pr1* expression (33, 34). Dual deficiency of Kdm6a and Kdm6b resulted in an exacerbated impediment of $CD4^+$ T cell egress, further indicating that Kdm6a and Kdm6b are not redundant and can have additive effects. Kdm6a and Kdm6b contain a Jumonji C catalytic domain on their C-terminal region, but their N-terminal domains are less conserved, suggesting the potential for other nonredundant functions [reviewed in (27)]. Indeed, it has been demonstrated that while Kdm6b modulates H3K27 methylation to promote NOTCH1 induced T cell acute lymphoblastic leukemia, Kdm6a functions as a tumor suppressor and is inactivated in this setting (31). However, the role of these lysine demethylases has not been evaluated jointly in $CD8^+$ T cell biology. Our studies demonstrate a Kdm6b-dependent chromatin remodeling of effector-associated gene loci, allowing for the proper generation and function of effector $CD8^+$ T cells. Similarly, Yamada et al. have also shown that Kdm6a (UTX) binds to *Pdrm1* loci and its deficiency impairs the removal of H3K27me3 from the 59 UTR, first exon and intron (29), highlighting the importance of Kdm6 family members in driving effector

CTL differentiation. However, Kdm6a-deficient cells have no defect upon recall responses (29) but we observe an impaired expansion of Kdm6b KO cells upon secondary challenge. Moreover, Kdm6a-deficient cells have normal expression of cytokines and Granzyme B, whereas our data shows that Kdm6b-deficient cells have defective granzyme and perforin expression, which correlates with decreased cytotoxicity function in vitro and in vivo. Yamada et al. were unable to observe any further differences in T cell responses upon treatment of Kdm6a-deficient cells with GSK-J4, an inhibitor targeting both Kdm6a and Kdm6b. This is surprising considering that our data clearly shows an important function of Kdm6b in driving effector CTL commitment, and the differences in phenotype between Kdm6a- and Kdm6b-deficient cells. Also, we have not observed any defects in $CD8^+$ T cell expansion upon Kdm6b deficiency at the peak of a primary immune response or during memory maintenance. However, reduced expansion of Ag-specific cells was observed upon secondary exposure to Ag. Further studies are needed to understand the kinetics and requirements of these lysine demethylases, and how they may function in redundant or specific manners to support effector CTL generation during primary and secondary responses.

Our data show that Kdm6b functions early during T cell activation to induce expression of effector-associated genes. We found that deficiency in Kdm6b results in impaired upregulation of effect- or-associated genes including *Tbx21*, which codes for T-bet, *Prdm1*, which codes for Blimp1, *Zeb2*, Granzymes A and B, and several killer cell lectin-like receptors (Klrs). It has been previously suggested that T-bet requires Kdm6b activity to promote expression of *Cxcr3* and *Ifng* in EL4 cells (63). Our results show that Kdm6b deficiency does not result in impaired IFN-γ production and in fact leads to increased levels of CXCR3 in vivo, suggesting that in $CD8^+$ T cells, Kdm6b might be dispensable for T-box family member activity. Moreover, despite no defects in CXCR3 or IFN-γ production, Kdm6b-deficient cells do show reduced T-bet expression at the peak of the immune response and at memory time points, suggesting that other T-box member or transcription factors might regulate the expression of these genes. A recently identified T-bet regulatory network shows the unique roles of T-bet in promoting the expression of *Zeb2*, *Gzma, Klrb1c* in the TE subset and *Bcl2*, *Crtam*, *Pou6f1* expression in the memory precursor subset respectively (64). Our RNA-seq data using acute deletion of Kdm6b in CTLs recapitulated the gene expression changes of the T-bet deficiency in the TE subset, suggesting that Kdm6b might hinder TE subset gene expression and function via T-bet regulatory network (Supplemental Fig. 4G). However, we were unable to observe reduced T-bet expression on d4 post infection, suggesting that other pathways may be important in further inducing T-bet expression during the expansion phase of CTLs after d4.

We identified discrepancies in the expression of T-bet and Eomes between the Kdm6b TKO mice model and the adoptive transfer model. The RNA-seq data from acute depletion of Kdm6b with shRNA (Fig. 4) and the P14 T cell adoptive transfer on day 29 (Fig. 3) consistently exhibit reduced T-bet and increased Eomes expression, which is different from the results observed upon infection of Kdm6b TKO mice. One possible explanation is an altered $CD4^+$ T helper signal in Kdm6b TKO mice, which might further result in phenotypic changes not observed upon acute deletion or adoptive transfer, both experimental setups that occur in the presence of WT $CD4^+$ T cells. In fact, our data showing defects in Tfh cell

generation in Kdm6b TKO mice supports these conclusions (36). Moreover, Kdm6b has been shown to bind to T-box protein to positively regulate Eomes expression in endoderm differentiation (65). Our data suggest Kdm6b is required for controlling the balance between T-bet and Eomes expression, resulting in the regulation of CTL differentiation. Further studies assessing the direct interaction of Kdm6b with specific lineage-determining transcription factors could provide more mechanistic insights into these regulatory gene networks.

Our data indicates that Kdm6b is an essential epigenetic regulator that induces chromatin accessibility in effector-associated genes early during infection. We identified that absence of Kdm6b results in increased expression of memory-associated genes, particularly central memory genes on d4 post infection (Fig. 6). Of interest, we observed reduced expression of *Il2ra* and *Il12rb1* on Kdm6b-deficient cells, and IL-2, together with IL-12 and type I IFNs have been shown to repress Tcf-1 expression, allowing for proper differentiation of effector CTLs (8, 38, 58, 59). We found that cells lacking Kdm6b preferentially give rise to Tcm cells, have higher expression of *Tcf7* (codes for Tcf-1) based on RNA-seq analysis and also show diminished cytotoxic activity. Consistent with this, Held and colleagues have recently demonstrated that cells expressing high levels of Tcf-1 during the effector phase of an acute viral infection give rise to the central memory pool and lack cytotoxic activity (66). Thus, these results suggest that Kdm6b indirectly represses central memory $CD8^+$ T cell generation through epigenetic chromatin remodeling of effector-associated genes. Another interesting finding was that Kdm6b deficiency resulted in defective expression of cytotoxic-related genes while not impacting cytokines such as IFN-$\gamma$ or TNF-$\alpha$. This suggests that the Kdm6b-dependent CTL effector program can be epigenetically regulated through distinct mechanisms.

Dynamic regulation of repressive histone marks is essential for the development of effector CTLs. Independent studies have shown that Ezh2, the catalytic subunit of PRC2, represses pro-memory and pro-survival genes through methylation of H3K27 residues, resulting in the proper differentiation of effector $CD8^+$ T cells. However, the initial repression of pro-memory genes during differentiation is not likely catalyzed by Ezh2 deposition of trimethylation marks given that Ezh2 deficiency in CTLs does not affect *Tcf7* and *Bach2* expression on day 4.5 p.i. (22, 26). Despite our observation of reduced initial repression of those pro-memory genes in Kdm6b-deficient CTLs, the exact mechanisms need further investigation. Our work also demonstrates the importance of removing H3K27me3 marks from effector-associated gene loci for the proper generation and function of effector CTLs. Moreover, recently the H3K9 methylase Suv39h1 has also been implicated in the repression of stemness genes to induce the generation of effector CD8 T cells (60). The exact cooperation between these different epigenetic modulators in vivo remains unclear. Future studies are needed to address whether the dynamic H3K9 or H3K27 methylation of distinct gene loci requires both marks simultaneously for gene repression and proper generation of effector CTLs.

In the current study, we demonstrate that Kdm6b acts as an epigenetic modulator of $CD8^+$ T cell fate determination by regulating effector-associated gene expression and chromatin accessibility. The exact role and potential cooperative nature between H3K27me3

lysine demethylases Kdm6a and Kdm6b needs further development. Because Kdm6 family members have been the therapeutic target for several cancers, properly understanding their intrinsic role in T cell function is warranted. Thus, our findings provide an important insight for the rational design of therapeutic strategies against infectious diseases, cancer, and autoimmunity.

## Supplementary Material

Refer to Web version on PubMed Central for supplementary material.

## Acknowledgments

We thank Robert Dickinson at Rosalind Franklin University of Medicine and Science Flow Cytometry Facility for help with cell sorting experiments, the La Jolla Institute Sequencing Facility for the assistance in sequencing our samples, the La Jolla Institute Bioinformatics Core for assistance in RNA-seq data analysis, and the National Institutes of Health Tetramer Facility for providing the LCMV tetramers described in the Materials and Methods.

This work was supported by a Rosalind Franklin University of Medicine and Science start-up fund (to G.J.M.) and supported in part by American Cancer Society Research Scholar Grant 131049-RSG-17–185-01-LIB (to G.J.M.). The La Jolla Institute NovaSeq 6000 instrument has been acquired through the Shared Instrumentation Grant Program (S10OD025052).

T.X. and G.J.M. designed the experiments and wrote the article. T.X. performed experiments, analyzed, and plotted the data. A.K. and A.S. maintained the mouse colony and helped with experiments. H.I.N., A.N.A.G., and L.J. performed the assay for transposase-accessible chromatin sequencing bioinformatics analysis. R.M.P. and M.E.P. provided valuable reagents and guidance in the project. G.J.M. supervised the project.

## Abbreviations used in this article:

| | |
|---|---|
| **ATAC-seq** | assay for transposase-accessible chromatin sequencing |
| **ChIP-seq** | chromatin immunoprecipitation sequencing |
| **d4** | day 4 |
| **d6** | day 6 |
| **d8** | day 8 |
| **d30** | day 30 |
| **d45** | day 45 |
| **Ezh2** | enhancer of zeste homolog 2 |
| **GSEA** | gene set enrichment analysis |
| **KO** | knockout |
| **LCMV** | lymphocytic choriomeningitis virus |
| **LCMV Arm** | LCMV Armstrong |
| **LM-gp33** | *L. monocytogenes*−GP33 |
| **MPEC** | memory precursor effector cell |

| | |
|---|---|
| **p.i.** | postinfection |
| **PRC2** | polycomb repressive complex 2 |
| **qPCR** | quantitative PCR |
| **RNA-seq** | RNA sequencing |
| **shRNA** | short hairpin RNA |
| **SLEC** | short-lived effector T cell |
| **Tcm** | central memory CTL |
| **TE** | terminal effector |
| **Tfh** | follicular helper T |
| **TKO** | T cell−specific KO |
| **Trm** | tissue resident memory $CD8^+$ T cell |
| **WT** | wild-type |

## References


1. Kaech SM, and Cui W. 2012. Transcriptional control of effector and memory CD8+ T cell differentiation. Nat. Rev. Immunol. 12: 749–761. [PubMed: 23080391]
2. Henning AN, Roychoudhuri R, and Restifo NP. 2018. Epigenetic control of $CD8^+$ T cell differentiation. Nat. Rev. Immunol. 18: 340–356. [PubMed: 29379213]
3. Weng NP, Araki Y, and Subedi K. 2012. The molecular basis of the memory T cell response: differential gene expression and its epigenetic regulation. Nat. Rev. Immunol. 12: 306–315. [PubMed: 22421787]
4. Zediak VP, Johnnidis JB, Wherry EJ, and Berger SL. 2011. Cutting edge: persistently open chromatin at effector gene loci in resting memory CD8+ T cells independent of transcriptional status. J. Immunol. 186: 2705–2709. [PubMed: 21278341]
5. Best JA, Blair DA, Knell J, Yang E, Mayya V, Doedens A, Dustin ML, and Goldrath AW; Immunological Genome Project Consortium. 2013. Transcriptional insights into the CD8(+) T cell response to infection and memory T cell formation. Nat. Immunol. 14: 404–412. [PubMed: 23396170]
6. Intlekofer AM, Takemoto N, Wherry EJ, Longworth SA, Northrup JT, Palanivel VR, Mullen AC, Gasink CR, Kaech SM, Miller JD, et al. 2005. Effector and memory CD8+ T cell fate coupled by T-bet and eomesodermin. [Published erratum appears in 2006 Nat. Immunol 7: 113.] Nat. Immunol. 6: 1236–1244. [PubMed: 16273099]
7. Banerjee A, Gordon SM, Intlekofer AM, Paley MA, Mooney EC, Lindsten T, Wherry EJ, and Reiner SL. 2010. Cutting edge: The transcription factor eomesodermin enables CD8+ T cells to compete for the memory cell niche. J. Immunol. 185: 4988–4992. [PubMed: 20935204]
8. Joshi NS, Cui W, Chandele A, Lee HK, Urso DR, Hagman J, Gapin L, and Kaech SM. 2007. Inflammation directs memory precursor and short-lived effector CD8(+) T cell fates via the graded expression of T-bet transcription factor. Immunity 27: 281–295. [PubMed: 17723218]
9. Cannarile MA, Lind NA, Rivera R, Sheridan AD, Camfield KA, Wu BB, Cheung KP, Ding Z, and Goldrath AW. 2006. Transcriptional regulator Id2 mediates CD8+ T cell immunity. Nat. Immunol. 7: 1317–1325. [PubMed: 17086188]

10. Ji Y, Pos Z, Rao M, Klebanoff CA, Yu Z, Sukumar M, Reger RN, Palmer DC, Borman ZA, Muranski P, et al. 2011. Repression of the DNA-binding inhibitor Id3 by Blimp-1 limits the formation of memory CD8+ T cells. Nat. Immunol. 12: 1230–1237. [PubMed: 22057288]
11. Yang CY, Best JA, Knell J, Yang E, Sheridan AD, Jesionek AK, Li HS, Rivera RR, Lind KC, D'Cruz LM, et al. 2011. The transcriptional regulators Id2 and Id3 control the formation of distinct memory CD8+ T cell subsets. Nat. Immunol. 12: 1221–1229. [PubMed: 22057289]
12. Xu T, Keller A, and Martinez GJ. 2019. NFAT1 and NFAT2 differentially regulate CTL differentiation upon acute viral infection. Front. Immunol. 10: 184. [PubMed: 30828328]
13. Ciofani M, Madar A, Galan C, Sellars M, Mace K, Pauli F, Agarwal A, Huang W, Parkhurst CN, Muratet M, et al. 2012. A validated regulatory network for Th17 cell specification. Cell 151: 289–303. [PubMed: 23021777]
14. Kurachi M, Barnitz RA, Yosef N, Odorizzi PM, DiIorio MA, Lemieux ME, Yates K, Godec J, Klatt MG, Regev A, et al. 2014. The transcription factor BATF operates as an essential differentiation checkpoint in early effector CD8+ T cells. Nat. Immunol. 15: 373–383. [PubMed: 24584090]
15. Wang D, Diao H, Getzler AJ, Rogal W, Frederick MA, Milner J, Yu B, Crotty S, Goldrath AW, and Pipkin ME. 2018. The transcription factor Runx3 establishes chromatin accessibility of cis-regulatory landscapes that drive memory cytotoxic T lymphocyte formation. Immunity 48: 659–674.e6. [PubMed: 29669249]
16. Milner JJ, Toma C, Yu B, Zhang K, Omilusik K, Phan AT, Wang D, Getzler AJ, Nguyen T, Crotty S, et al. 2017. Runx3 programs $CD8^+$ T cell residency in non-lymphoid tissues and tumours. [Published erratum appears in 2017 Nature 554: 392.] Nature 552: 253–257. [PubMed: 29211713]
17. Rutishauser RL, and Kaech SM. 2010. Generating diversity: transcriptional regulation of effector and memory CD8 T-cell differentiation. Immunol. Rev. 235: 219–233. [PubMed: 20536566]
18. Schmidl C, Delacher M, Huehn J, and Feuerer M. 2018. Epigenetic mechanisms regulating T-cell responses. J. Allergy Clin. Immunol. 142: 728–743. [PubMed: 30195378]
19. Kouzarides T 2007. Chromatin modifications and their function. Cell 128: 693–705. [PubMed: 17320507]
20. Black JC, Van Rechem C, and Whetstine JR. 2012. Histone lysine methylation dynamics: establishment, regulation, and biological impact. Mol. Cell 48: 491–507. [PubMed: 23200123]
21. Voigt P, Tee WW, and Reinberg D. 2013. A double take on bivalent promoters. Genes Dev. 27: 1318–1338. [PubMed: 23788621]
22. Gray SM, Amezquita RA, Guan T, Kleinstein SH, and Kaech SM. 2017. Polycomb repressive complex 2-mediated chromatin repression guides effector $CD8^+$ T cell terminal differentiation and loss of multipotency. Immunity 46: 596–608. [PubMed: 28410989]
23. Russ BE, Olshanksy M, Smallwood HS, Li J, Denton AE, Prier JE, Stock AT, Croom HA, Cullen JG, Nguyen ML, et al. 2014. Distinct epigenetic signatures delineate transcriptional programs during virus-specific CD8(+) T cell differentiation. [Published erratum appears in 2014 Immunity 41: 1064.] Immunity 41: 853–865. [PubMed: 25517617]
24. Russ BE, Olshansky M, Li J, Nguyen MLT, Gearing LJ, Nguyen THO, Olson MR, McQuilton HA, Nüssing S, Khoury G, et al. 2017. Regulation of H3K4me3 at transcriptional enhancers characterizes acquisition of virus-specific $CD8^+$ T cell-lineage-specific function. Cell Rep. 21: 3624–3636. [PubMed: 29262339]
25. Scott-Browne JP, López-Moyado IF, Trifari S, Wong V, Chavez L, Rao A, and Pereira RM. 2016. Dynamic changes in chromatin accessibility occur in $CD8^+$ T cells responding to viral infection. Immunity 45: 1327–1340. [PubMed: 27939672]
26. Kakaradov B, Arsenio J, Widjaja CE, He Z, Aigner S, Metz PJ, Yu B, Wehrens EJ, Lopez J, Kim SH, et al. 2017. Early transcriptional and epigenetic regulation of $CD8^+$ T cell differentiation revealed by single-cell RNA sequencing. Nat. Immunol. 18: 422–432. [PubMed: 28218746]
27. Johansson C, Tumber A, Che K, Cain P, Nowak R, Gileadi C, and Oppermann U. 2014. The roles of Jumonji-type oxygenases in human disease. Epigenomics 6: 89–120. [PubMed: 24579949]
28. Hong S, Cho YW, Yu LR, Yu H, Veenstra TD, and Ge K. 2007. Identification of JmjC domain-containing UTX and JMJD3 as histone H3 lysine 27 demethylases. Proc. Natl. Acad. Sci. USA 104: 18439–18444. [PubMed: 18003914]

29. Yamada T, Nabe S, Toriyama K, Suzuki J, Inoue K, Imai Y, Shiraishi A, Takenaka K, Yasukawa M, and Yamashita M. 2019. Histone H3K27 demethylase negatively controls the memory formation of antigen-stimulated $CD8^+$ T cells. J. Immunol. 202: 1088–1098. [PubMed: 30626691]
30. Yang L, Song L, Liu X, Bai L, and Li G. 2018. KDM6A and KDM6B play contrasting roles in nuclear transfer embryos revealed by MERVL reporter system. EMBO Rep. 19: e46240.
31. Ntziachristos P, Tsirigos A, Welstead GG, Trimarchi T, Bakogianni S, Xu L, Loizou E, Holmfeldt L, Strikoudis A, King B, et al. 2014. Contrasting roles of histone 3 lysine 27 demethylases in acute lymphoblastic leukaemia. Nature 514: 513–517. [PubMed: 25132549]
32. Northrup D, Yagi R, Cui K, Proctor WR, Wang C, Placek K, Pohl LR, Wang R, Ge K, Zhu J, and Zhao K. 2017. Histone demethylases UTX and JMJD3 are required for NKT cell development in mice. Cell Biosci. 7: 25. [PubMed: 28529687]
33. Fu C, Li Q, Zou J, Xing C, Luo M, Yin B, Chu J, Yu J, Liu X, Wang HY, and Wang RF. 2019. JMJD3 regulates CD4 T cell trafficking by targeting actin cytoskeleton regulatory gene Pdlim4. J. Clin. Invest. 129: 4745–4757. [PubMed: 31393857]
34. Manna S, Kim JK, Baugé C, Cam M, Zhao Y, Shetty J, Vacchio MS, Castro E, Tran B, Tessarollo L, and Bosselut R. 2015. Histone H3 Lysine 27 demethylases Jmjd3 and Utx are required for T-cell differentiation. Nat. Commun. 6: 8152. [PubMed: 26328764]
35. Cribbs AP, Terlecki-Zaniewicz S, Philpott M, Baardman J, Ahern D, Lindow M, Obad S, Oerum H, Sampey B, Mander PK, et al. 2020. Histone H3K27me3 demethylases regulate human Th17 cell development and effector functions by impacting on metabolism. Proc. Natl. Acad. Sci. USA 117: 6056–6066. [PubMed: 32123118]
36. Li Q, Zou J, Wang M, Ding X, Chepelev I, Zhou X, Zhao W, Wei G, Cui J, Zhao K, et al. 2014. Critical role of histone demethylase Jmjd3 in the regulation of CD41 T-cell differentiation. Nat. Commun. 5: 5780. [PubMed: 25531312]
37. Martinez GJ, Hu JK, Pereira RM, Crampton JS, Togher S, Bild N, Crotty S, and Rao A. 2016. Cutting Edge: NFAT transcription factors promote the generation of follicular helper T cells in response to acute viral infection. J. Immunol. 196: 2015–2019. [PubMed: 26851216]
38. Pipkin ME, Sacks JA, Cruz-Guilloty F, Lichtenheld MG, Bevan MJ, and Rao A. 2010. Interleukin-2 and inflammation induce distinct transcriptional programs that promote the differentiation of effector cytolytic T cells. Immunity 32: 79–90. [PubMed: 20096607]
39. Chen R, Bélanger S, Frederick MA, Li B, Johnston RJ, Xiao N, Liu YC, Sharma S, Peters B, Rao A, et al. 2014. In vivo RNA interference screens identify regulators of antiviral CD4(+) and CD8(+) T cell differentiation. Immunity 41: 325–338. [PubMed: 25148027]
40. Crotty S, McCausland MM, Aubert RD, Wherry EJ, and Ahmed R. 2006. Hypogammaglobulinemia and exacerbated CD8 T-cell-mediated immunopathology in SAP-deficient mice with chronic LCMV infection mimics human XLP disease. Blood 108: 3085–3093. [PubMed: 16788096]
41. Wherry EJ, Blattman JN, Murali-Krishna K, van der Most R, and Ahmed R. 2003. Viral persistence alters CD8 T-cell immunodominance and tissue distribution and results in distinct stages of functional impairment. J. Virol. 77: 4911–4927. [PubMed: 12663797]
42. Olson JA, McDonald-Hyman C, Jameson SC, and Hamilton SE. 2013. Effector-like $CD8^+$ T cells in the memory population mediate potent protective immunity. Immunity 38: 1250–1260. [PubMed: 23746652]
43. Dobin A, Davis CA, Schlesinger F, Drenkow J, Zaleski C, Jha S, Batut P, Chaisson M, and Gingeras TR. 2012. STAR: ultrafast universal RNA-seq aligner. Bioinformatics 29: 15–21. [PubMed: 23104886]
44. Schmieder R, and Edwards R. 2011. Quality control and preprocessing of metagenomic datasets. Bioinformatics 27: 863–864. [PubMed: 21278185]
45. Li H, Handsaker B, Wysoker A, Fennell T, Ruan J, Homer N, Marth G, Abecasis G, and Durbin R; 1000 Genome Project Data Processing Subgroup. 2009. The sequence alignment/map format and SAMtools. Bioinformatics 25: 2078–2079. [PubMed: 19505943]
46. Liao Y, Smyth GK, and Shi W. 2013. featureCounts: An efficient general purpose program for assigning sequence reads to genomic features. Bioinformatics 30: 923–930. [PubMed: 24227677]

47. Love MI, Huber W, and Anders S. 2014. Moderated estimation of fold change and dispersion for RNA-seq data with DESeq2. Genome Biol. 15: 550. [PubMed: 25516281]
48. Benjamini Y, and Hochberg Y. 1995. Controlling the false discovery rate: a practical and powerful approach to multiple testing. J. R. Stat. Soc Series B Stat Methodol. 57: 289–300.
49. Buenrostro JD, Giresi PG, Zaba LC, Chang HY, and Greenleaf WJ. 2013. Transposition of native chromatin for fast and sensitive epigenomic profiling of open chromatin, DNA-binding proteins and nucleosome position. Nat. Methods 10: 1213–1218. [PubMed: 24097267]
50. Langmead B, Trapnell C, Pop M, and Salzberg SL. 2009. Ultrafast and memory-efficient alignment of short DNA sequences to the human genome. Genome Biol. 10: R25. [PubMed: 19261174]
51. Zhang Y, Liu T, Meyer CA, Eeckhoute J, Johnson DS, Bernstein BE, Nusbaum C, Myers RM, Brown M, Li W, and Liu XS. 2008. Model-based analysis of ChIP-Seq (MACS). Genome Biol. 9: R137. [PubMed: 18798982]
52. Quinlan AR, and Hall IM. 2010. BEDTools: a flexible suite of utilities for comparing genomic features. Bioinformatics 26: 841–842. [PubMed: 20110278]
53. Lee S, Lee JW, and Lee SK. 2012. UTX, a histone H3-lysine 27 demethylase, acts as a critical switch to activate the cardiac developmental program. Dev. Cell 22: 25–37. [PubMed: 22192413]
54. Li Q, Wang HY, Chepelev I, Zhu Q, Wei G, Zhao K, and Wang RF. 2014. Stage-dependent and locus-specific role of histone demethylase Jumonji D3 (JMJD3) in the embryonic stages of lung development. PLoS Genet. 10: e1004524.
55. Cook KD, Shpargel KB, Starmer J, Whitfield-Larry F, Conley B, Allard DE, Rager JE, Fry RC, Davenport ML, Magnuson T, et al. 2015. T follicular helper cell-dependent clearance of a persistent virus infection requires T cell expression of the histone demethylase UTX. Immunity 43: 703–714. [PubMed: 26431949]
56. Martinez GJ, Pereira RM, A€ ij€o T, Kim EY, Marangoni F, Pipkin ME, Togher S, Heissmeyer V, Zhang YC, Crotty S, et al. 2015. The transcription factor NFAT promotes exhaustion of activated $CD8^+$ T cells. Immunity 42: 265–278. [PubMed: 25680272]
57. Herndler-Brandstetter D, Ishigame H, Shinnakasu R, Plajer V, Stecher C, Zhao J, Lietzenmayer M, Kroehling L, Takumi A, Kometani K, et al. 2018. $KLRG1^+$ effector $CD8^+$ T cells lose KLRG1, differentiate into all memory T cell lineages, and convey enhanced protective immunity. Immunity 48: 716–729.e8. [PubMed: 29625895]
58. Danilo M, Chennupati V, Silva JG, Siegert S, and Held W. 2018. Suppression of Tcf1 by inflammatory cytokines facilitates effector CD8 T cell differentiation. Cell Rep. 22: 2107–2117. [PubMed: 29466737]
59. Keppler SJ, Rosenits K, Koegl T, Vucikuja S, and Aichele P. 2012. Signal 3 cytokines as modulators of primary immune responses during infections: the interplay of type I IFN and IL-12 in CD8 T cell responses. PLoS One 7: e40865.
60. Pace L, Goudot C, Zueva E, Gueguen P, Burgdorf N, Waterfall JJ, Quivy JP, Almouzni G, and Amigorena S. 2018. The epigenetic control of stemness in $CD8^+$ T cell fate commitment. Science 359: 177–186. [PubMed: 29326266]
61. Ladle BH, Li KP, Phillips MJ, Pucsek AB, Haile A, Powell JD, Jaffee EM, Hildeman DA, and Gamper CJ. 2016. De novo DNA methylation by DNA methyltransferase 3a controls early effector CD8+ T-cell fate decisions following activation. Proc. Natl. Acad. Sci. USA 113: 10631–10636. [PubMed: 27582468]
62. Youngblood B, Hale JS, Kissick HT, Ahn E, Xu X, Wieland A, Araki K, West EE, Ghoneim HE, Fan Y, et al. 2017. Effector CD8 T cells dedifferentiate into long-lived memory cells. Nature 552: 404–409. [PubMed: 29236683]
63. Miller SA, Mohn SE, and Weinmann AS. 2010. Jmjd3 and UTX play a demethylase-independent role in chromatin remodeling to regulate T-box family member-dependent gene expression. Mol. Cell 40: 594–605. [PubMed: 21095589]
64. Yu B, Zhang K, Milner JJ, Toma C, Chen R, Scott-Browne JP, Pereira RM, Crotty S, Chang JT, Pipkin ME, et al. 2017. Epigenetic landscapes reveal transcription factors that regulate $CD8^+$ T cell differentiation. [Published erratum appears in 2017 Nat. Immunol 18: 705.] Nat. Immunol. 18: 573–582. [PubMed: 28288100]

65. Kartikasari AE, Zhou JX, Kanji MS, Chan DN, Sinha A, Grapin-Botton A, Magnuson MA, Lowry WE, and Bhushan A. 2013. The histone demethylase Jmjd3 sequentially associates with the transcription factors Tbx3 and Eomes to drive endoderm differentiation. EMBO J. 32: 1393–1408. [PubMed: 23584530]

66. Pais Ferreira D, Silva JG, Wyss T, Fuertes Marraco SA, Scarpellino L, Charmoy M, Maas R, Siddiqui I, Tang L, Joyce JA, et al. 2020. Central memory $CD8^+$ T cells derive from stem-like $Tcf7^{hi}$ effector cells in the absence of cytotoxic differentiation. Immunity 53: 985–1000.e11. [PubMed: 33128876]

67. Yu G, Wang LG, Han Y, and He QY. 2012. clusterProfiler: An R package for comparing biological themes among gene clusters. OMICS 16: 284–287. [PubMed: 22455463]

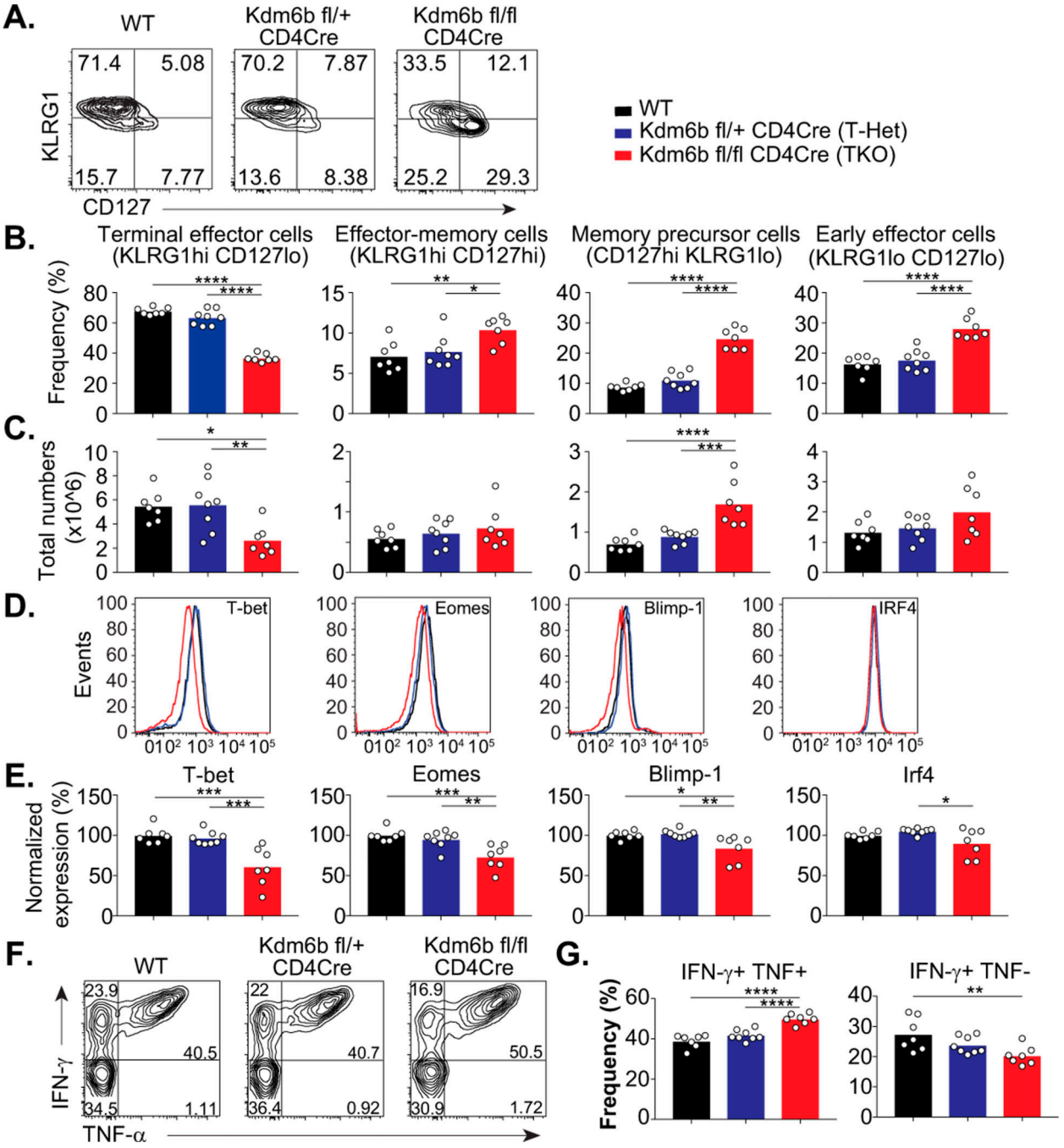


**FIGURE 1.**

Kdm6b is required for effector CD8$^{+}$ T cell differentiation at the peak of the T cell expansion phase during an acute viral infection. Kdm6b$^{fl/fl}$ CD4Cre (TKO), Kdm6b$^{fl/+}$ CD4Cre (T-Het), or WT mice were infected with LCMV Arm. Splenocytes were characterized at d8 p.i. (**A**–**C**) Representative specific cells determined by the expression of KLRG1 and CD127 (A) or the summary data of both frequency (B) and total numbers (C). (**D** and **E**) Expression of transcription factors T-bet, Eomes, Blimp-1, and IRF4 on CD4$^{-}$ CD8$^{+}$ CD44$^{hi}$ H2D -gp$_{33–41}$$^{+}$ was determined by intracellular staining as a representative

histogram (D) or the combined normalized expression (E). (**F** and **G**) Splenocytes were restimulated with gp33–41 peptide for 4hrs in the presence of brefeldin A, and intracellular cytokine staining was performed. Representative contour plot (F) and combined frequency (G) of IFN-γ and TNF-α expression. The combined data of two independent experiments is shown. Statistical analysis was done with data from two biological replicates using nonpaired one-way ANOVA followed by Tukey multiple comparisons. *$p \leq 0.05$, **$p \leq 0.01$, ***$p \leq 0.001$, ****$p \leq 0.0001$. See Supplemental Fig 1.

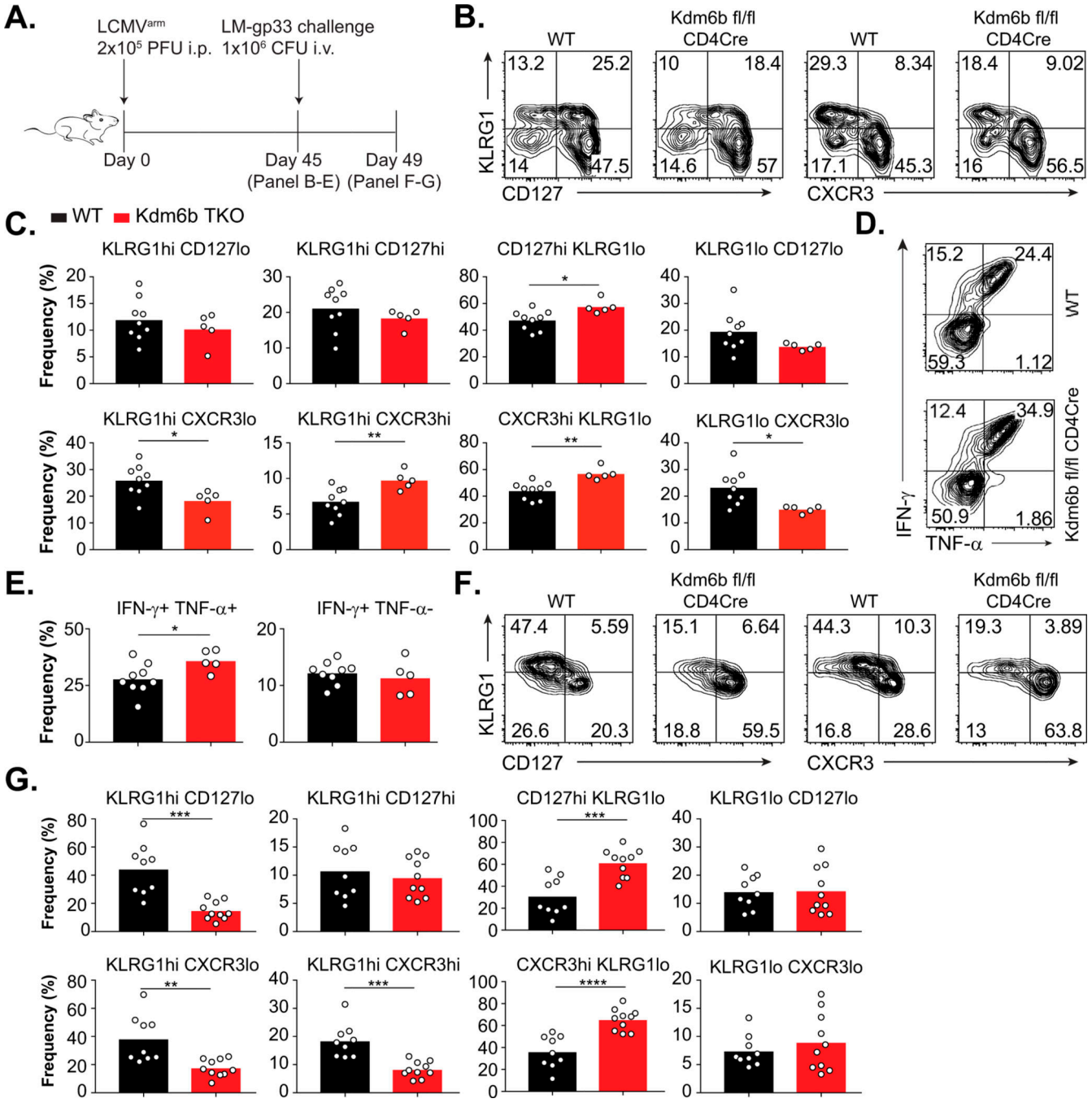


**FIGURE 2.**

Impaired recall response upon Kdm6b deficiency despite enhanced memory cell generation. Kdm6b$^{fl/fl}$ CD4Cre (TKO) or WT mice were infected with LCMV Arm, and splenic CD8$^{+}$ T cell population characterized on d45 p.i. (**A**–**E**). On d45, a subset of mice was challenged with *L. monocytogenes* expressing gp33–41, and splenocytes characterized 4 d later (**F** and **G**). (A) Schematics of the experimental design. (B and C) Representative flow contour plot of CD4$^{-}$ CD8$^{+}$ CD44$^{hi}$ H2D$^{b}$-gp$_{33–41}$[2] Ag-specific cells determined by the expression of KLRG1, CD127, and CXCR3 (B and F) or the summary data of frequency of the indicated

populations (C and G). (D and E) Representative contour plot (D) and combined frequency (E) of IFN-γ and TNF-α expression. The combined data of two independent experiments is shown. Student *t* test was performed to analyze statistical differences between groups from two biological replicates. *$p \leq 0.05$, **$p \leq 0.01$, ***$p \leq 0.001$, ****$p \leq 0.0001$. See Supplemental Fig. 2.

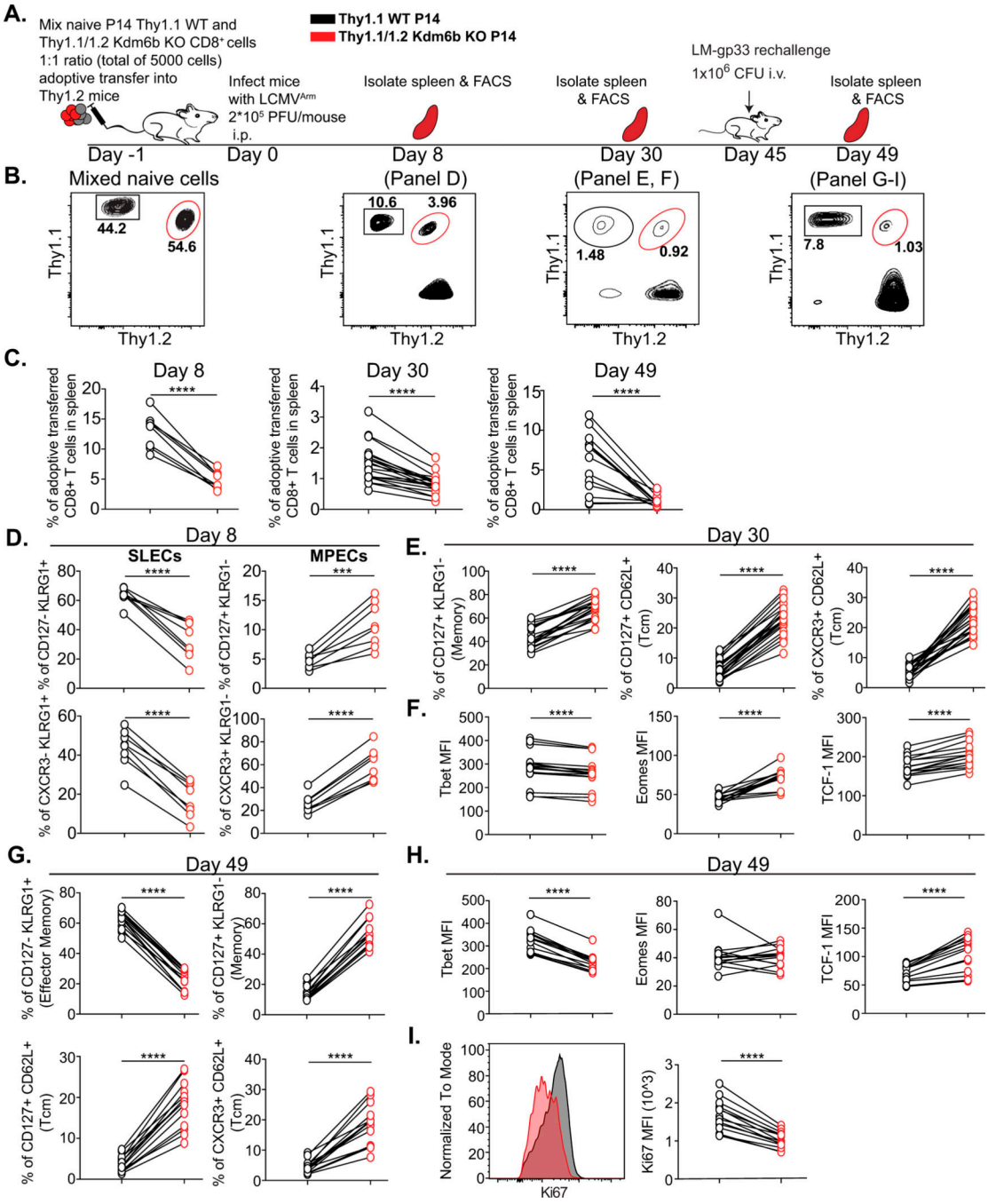


**FIGURE 3.**

Cell-intrinsic regulation of central memory CTL differentiation by Kdm6b. Naive WT (Thy1.1) and Kdm6b KO (Thy1.1/Thy1.2) P14 TCR-transgenic CD8+ T cells were mixed 1:1 and transferred into C57BL/6 congenic (Thy1.2) mice, after which mice were infected with LCMV Arm. At different time points, cells were characterized. On d45, mice were challenged with *L. monocytogenes* expressing gp33–41 (LM-gp33), and mice euthanized 4d later. (**A**) Schematic representation of the experimental design and execution. (**B**) Contour plots showing the frequency of WT (Thy1.1$^+$) and Kdm6b KO (Thy1.1$^+$ Thy1.2$^+$) P14 CD8$^+$

T cells at different time points. (**C**) Percentage of adoptive transferred WT (black) or Kdm6b KO (red) $CD8^+$ T cells at indicated time points. (**D**, **E**, and **G**) Percentage of WT and Kdm6b KO $CD8^+$ T cells based on expression of KLRG1, CD127, CD62L and/or CXCR3 on d8 (D), d30 (E) post LCMV infection, or post rechallenge with LM-gp33 (day 49 [d49]) (G). (E−G) Characterization of adoptive transferred WT or Kdm6b KO $CD8^+$ T cells over 30 days p.i. (**F** and **H**) Expression (geometric mean fluorescence intensity) of transcription factors T-bet, Eomes, and TCF-1 from adoptive transferred WT or Kdm6b KO $CD8^+$ T cells on d30 (F) or d49 (H). (**I**) Expression of Ki67 on WT or Kdm6b KO cells on d49. Data were collected from two independent experiments and two-tail paired *t* tests were used for statistical analysis. Lines connecting dots represent an individual mouse. ****$p \leq 0.0001$. See Supplemental Fig. 3.

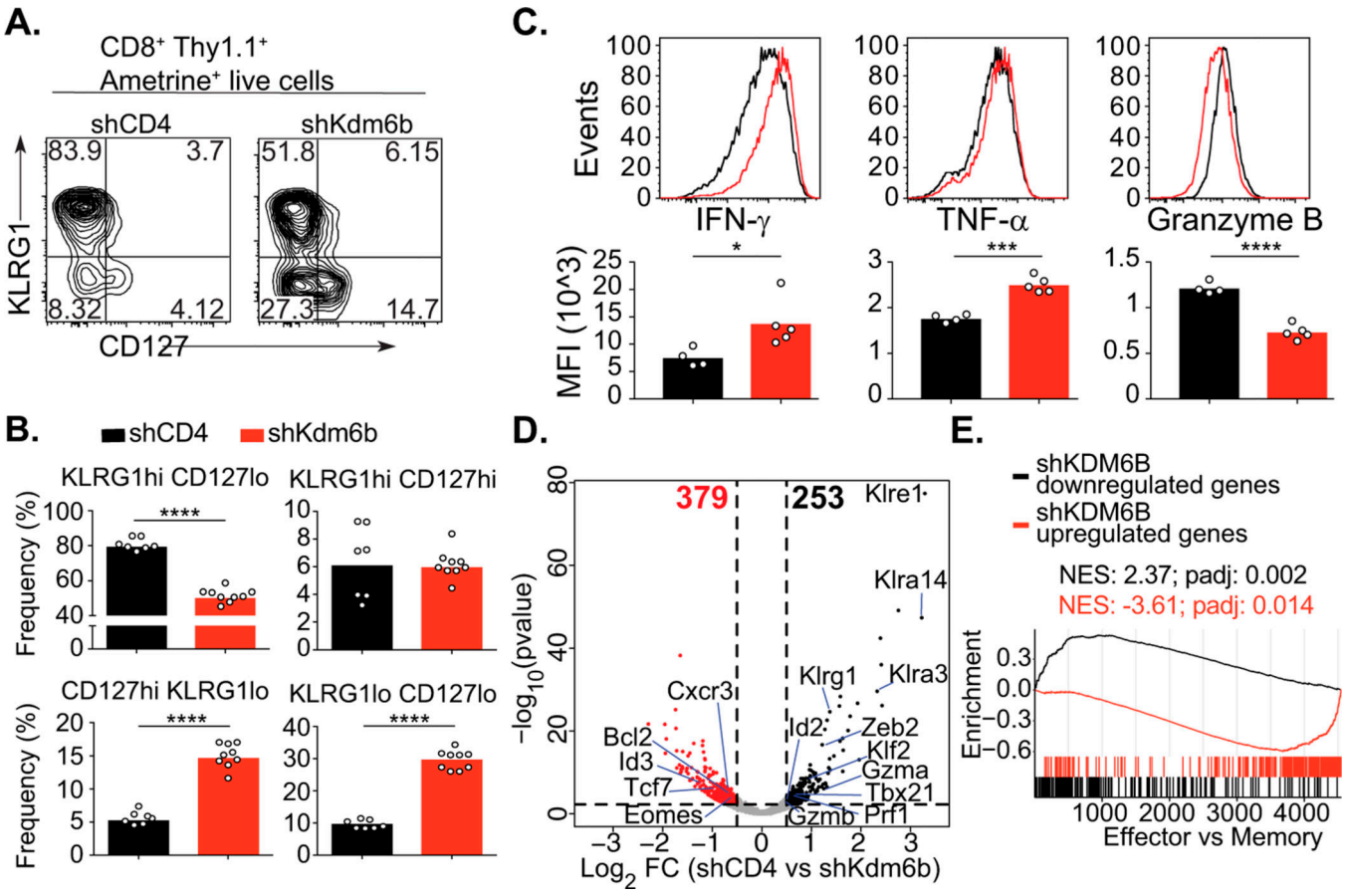


**FIGURE 4.**

Acute Kdm6b deficiency in CD8$^+$ T cells results in the defective effector-associated transcriptional program. P14 Thy1.1$^+$ CD8$^+$ T cells were transduced with shCD4 or shKdm6b and adoptively-transferred into congenic C57BL/6 (Thy1.2$^+$) mice, which was subsequently infected with LCMV cl13 ($1.5 \times 10^5$ PFU/mouse). Eight days p.i., splenocytes were harvested and adoptively transferred and transduced CD8$^+$ T cells were further gated for phenotypic characterization and sorted for RNA-seq and qPCR analysis. (**A** and **B**) Representative flow contour plot of CD8$^+$ Thy1.1$^+$ Ametrine$^{hi}$ cells determined by the expression of KLRG1 and CD127 (A) or the summary data of frequency of the indicated populations from three independent experiments (B). (**C**) Splenocytes were restimulated with gp33–41 peptide for 4hrs in the presence of brefeldin A, and intracellular cytokine staining was performed. A representative histogram is shown on the top panel and the combined frequency in the bottom panel for each cytokine. A representative of three independent experiments is shown. (**D** and **E**) RNA-seq was performed on total CD8$^+$ P14 Thy1.1$^+$ Ametrine$^{hi}$ cells. (D) Volcano plot displaying the differentially expressed genes with $p_{adj} < 0.05$ and $Log_2FC > 0.5$ cutoff comparing shCD4 control and shKdm6b knockdown from RNA-seq. Differentially expressed genes with the cut-off are labeled at the top. (E) GSEA and normalized enrichment scores (NES) of preranked transcriptional signatures associated with effector or memory cells (25) compared with all differentially expressed genes ($P_{adj} < 0.05$) in shCD4 versus shKdm6b using clusterProfiler (67). Student

*t* tests were performed for statistical analysis. *$p \leq 0.05$, **$p \leq 0.01$, ***$p \leq 0.001$, ****$p \leq 0.0001$. See Supplemental Fig. 4.

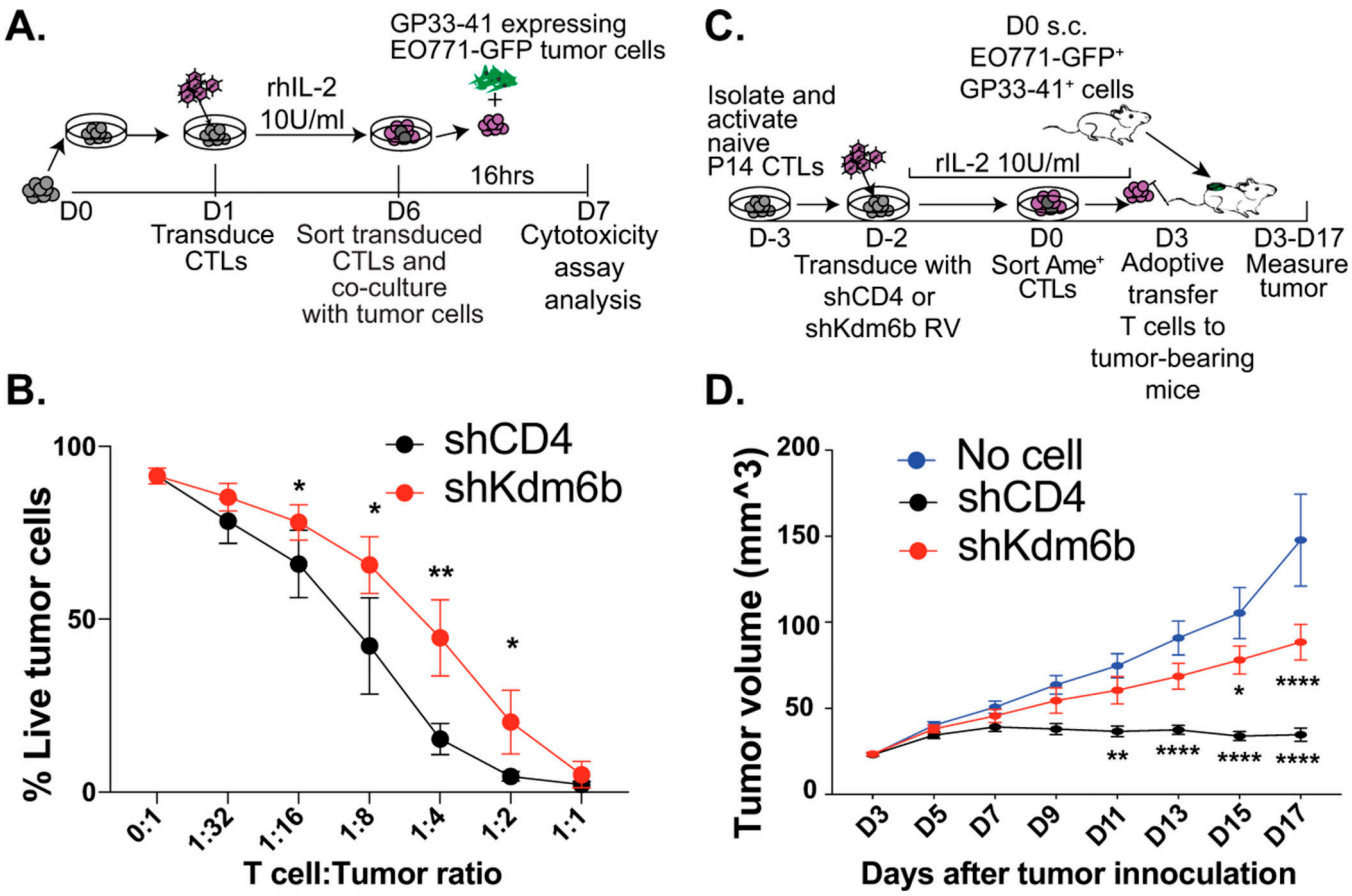


**FIGURE 5.**

Kdm6b is cell-intrinsically indispensable for proper cytotoxic activity in CTLs. (**A** and **B**) Naive P14 $CD8^+$ T cells were activated in vitro with anti-CD3 and anti-CD28 and transduced with retroviral constructs expressing shCD4 or shKdm6b. Cells were then cultured under memory-like conditions (38). On d6, $Ametrine^{hi}$ cells were FACS-purified and cultured at indicated ratios with EO771-GFP $gp_{33–41}{}^+$ target cells for 18 h. The percentage of $GFP^+$ live tumor cells was determined as an indication of cytotoxicity. (A) Schematics of the experimental design. (B) Line and dot plot show the cytotoxicity of transduced cells at different dilutions with mean $^{+/-}$ SD from four independent experiments. Statistics were performed using a two-way ANOVA followed by Dunnett comparisons. (**C** and **D**) Naive P14 $CD8^+$ T cells were transduced as in (A) but $Ametrine^{hi}$ cells were FACS-purified on d3 and further expanded until d6 in vitro. Cells were then transferred into EO771-GFP-gp33–41 tumor-bearing mice. (C) Schematics of experimental design. (D) Tumor growth kinetics of mice that did not receive any cells (blue line), mice that receive shCD4-transduced control cells (black line) or mice that received shKdm6b-expressing cells (redline). Statistics were performed using a one-way ANOVA followed by Tukey multiple comparisons. $*p \leq 0.05$, $**p \leq 0.01$, $****p \leq 0.0001$. See Supplemental Fig. 5.

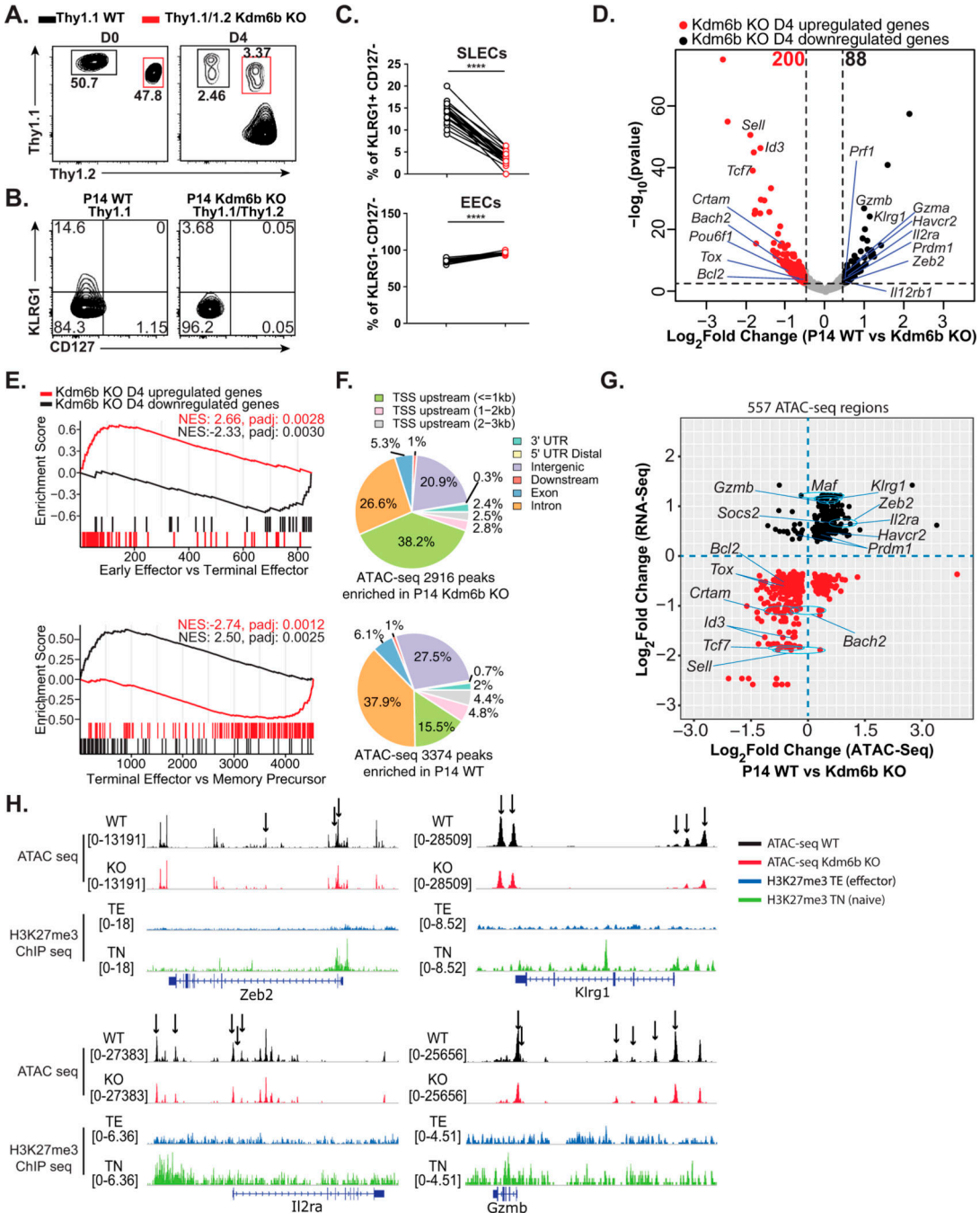


**FIGURE 6.**

Kdm6b is epigenetically required for promoting effector-associated genes and restraining EEC and memory precursor early during T cell differentiation. Naive WT (Thy1.1) and Kdm6b KO (Thy1.1/Thy1.2) P14 TCR-transgenic $CD8^+$ T cells were mixed 1:1 and transferred into C57BL/6 congenic (Thy1.2) mice, after which mice were infected with LCMV Arm. Four days p.i. WT and Kdm6b KO $CD8^+$ T cells were phenotypically characterized and sorted for RNA-seq and ATAC-seq. (**A**) Representative flow plot showing the WT ($Thy1.1^+$) and Kdm6b KO ($Thy1.1^+$ $Thy1.2^+$) P14 T cells on day 0 prior to

transfer and on d4 p.i. (**B** and **C**). Representative and combined percentage of KLRG1 and CD127 expression that determine SLEC ($KLRG1^+$ $CD127^-$) and EEC ($KLRG1^-$ $CD127^-$) populations. (**D**) Volcano plot showing differentially expressed genes with $p_{adj} < 0.05$ and $Log_2FC > 0.5$ cutoff by comparing P14 WT and Kdm6b KO cells. Genes of interest are labeled, and the number of differentially-expressed genes depicted. (**E**) GSEA and normalized enrichment scores (NES) of differentially expressed genes ($p_{adj} < 0.05$) in preranked transcriptional signatures of EEC, TE or memory precursor datasets obtained from (15). (**F**) Genomic distribution of differentially accessible regions determined by ATAC-seq (FDR < 0.05). (**G**) Correlation of differentially expressed genes (*y*-axis) and chromatin accessible regions of the different gene loci (*x*-axis) between WT and Kdm6b-deficient cells. Genes of interest are labeled; multiple differential accessible regions are circled out. (**H**) Representative gene loci showing the ATAC-seq peaks identified in WT and Kdm6b KO cells, and published H3K27me3 ChIP-seq from (26). Data were collected from three independent experiments and two-tail paired *t* tests were used for statistical analysis. Lines connecting dots represent an individual mouse. Three biological replicates were used for next generation sequencing. ****$p \leq 0.0001$. See Supplemental Fig. 6.